HHS Public Access

Author manuscript

ACS Appl Bio Mater. Author manuscript; available in PMC 2024 August 21.

Published in final edited form as:

ACS Appl Bio Mater. 2023 August 21; 6(8): 3199–3212. doi:10.1021/acsabm.3c00320.

Highly Sensitive Cyanine Dyes for Rapid Sensing of NAD(P)H in Mitochondria and First-instar Larvae of *Drosophila melanogaster*

Dilka Liyana Arachchige,
Department of Chemistry, and Health Research Institute, Michigan Technological University, Houghton, MI 49931.

Sushil K. Dwivedi,
Department of Chemistry, and Health Research Institute, Michigan Technological University, Houghton, MI 49931.

Sophia Jaeger,
Department of Chemistry, and Health Research Institute, Michigan Technological University, Houghton, MI 49931.

Adenike Mary Olowolagba,
Department of Chemistry, and Health Research Institute, Michigan Technological University, Houghton, MI 49931.

Mohamed Mahmoud,
Department of Chemistry, and Health Research Institute, Michigan Technological University, Houghton, MI 49931.

Daniel R. Tucker,
Department of Chemistry, and Health Research Institute, Michigan Technological University, Houghton, MI 49931.

Delaney Raine Fritz,
Department of Biological Sciences, and Health Research Institute, Michigan Technological University, Houghton, MI 49931.

Thomas Werner,
Department of Biological Sciences, and Health Research Institute, Michigan Technological University, Houghton, MI 49931.

Marina Tanasova,

Corresponding authors hyliu@mtu.edu, rluck@mtu.edu.

Author Contributions

R.L. Luck and H.Y. Liu contributed to conceptualization, methodology, manuscript writing, project administration, supervision, and funding acquisition. S. K. Dwivedi, D. L. Arachchige, S. Jaeger, A. M. Olowolagba, and M. Mahmoud were involved in investigation and data analysis. R.L. Luck and D. R. Tucker handled the computation chemistry of fluorescent probes. D. R. Fritz and T. Werner were responsible for fluorescence imaging of the fruit fly. M. Tanasova provided the normal cell line and guided the team on cell culture techniques using the normal cell line.

ASSOCIATE CONTENT

Supporting Information is available free of charge, and it includes NMR and MS spectra of the probes, MS spectra of the probe reaction products, computation results of the probes and their reaction products, and probe photostability and cytotoxicity.

The authors have no financial conflicts of interest to declare.

Department of Chemistry, and Health Research Institute, Michigan Technological University, Houghton, MI 49931.

Rudy L Luck,
Department of Chemistry, Michigan Technological University, Houghton, MI 49931.

Haiying Liu
Department of Chemistry, and Health Research Institute, Michigan Technological University, Houghton, MI 49931.

Abstract

We have developed two highly sensitive cyanine dyes, which we refer to as probes **A** and **B**. These dyes are capable of quick and sensitive sensing of NAD(P)H. The dyes were fabricated by connecting benzothiazolium and 2,3-dimethylnaphtho[1,2-d]thiazol-3-ium units to 3-quinolinium through a vinyl bond. In the absence of NAD(P)H, both probes have low fluorescence and absorption peaks at 370 nm and 400 nm, correspondingly. This is because of their two electron-withdrawing acceptor systems with highly positive charge densities. However, when NAD(P)H reduces the probe's electron-withdrawing 3-quinolinium units to electron-donating 1,4-dihydroquinoline units, the probes absorb at 533 nm and 535 nm and fluoresce at 572 nm and 586 nm for **A** and **B** correspondingly. This creates well-defined donor-π-acceptor cyanine dyes. We successfully used probe **A** to monitor NAD(P)H levels in live cells during glycolysis, under hypoxic conditions induced by $CoCl_2$ treatment, and after treatment with cancer drugs, including cisplatin, camptothecin, and gemcitabine. Probe **A** was also employed to visualize NADH in *Drosophila melanogaster* first-instar larvae. We observed an increase in NAD(P)H levels in A549 cancer cells both under hypoxic conditions and after treatment with cancer drugs, including cisplatin, camptothecin, and gemcitabine.

Keywords

NAD(P)H; Fluorescent Probe; Mitochondria; Cyanine Dye; Fluorescence Imaging

INTRODUCTION

NAD^+ and $NADP^+$ are coenzymes involved in redox reactions in eukaryotic cells, including cellular metabolism and various processes.[1–3] The reduced forms, NADH and NADPH, respectively, maintain cellular redox homeostasis and modulate biological events.[1–3] Imbalances or deficiencies in these redox couples are associated with pathological disorders.[4, 5] They are also involved in several redox reactions, such as energy metabolism, gluconeogenesis, oxidative phosphorylation, glycolysis, and the tricarboxylic acid cycle, as well as various cellular processes, including calcium homeostasis, oxidative stress, gene repair, mitochondrial functions, embryonic development, immune function, transcription, cell cycle, cell death, cellular senescence, hypoglycemia, apoptosis, hypoxia, and virus infections.[1–5] Detecting NAD(P)H concentrations is crucial for understanding physiological developments and pathological mechanisms. Assessing NAD(P)H levels in live cells provides valuable insights into cellular redox homeostasis and modulates biological events. Measuring the concentration of NAD(P)H in cancer cells after administering various drugs

is also important for understanding drug action and resistance, developing new treatments, and monitoring treatment effectiveness. [6–25] Fluorescence methods offer unique advantages for real-time visualization of NAD(P)H in live cells, including sensitivity, selectivity, rapid responses, simple operations, and spatiotemporal resolution (Table S1 in supporting information).[6–25]

Two cyanine-based molecules, probes **A** and **B**, were developed to determine NAD(P)H levels (Scheme 1). Probes **A** and **B** consist of a double connection bridge between 3-quinolinium and benzothiazolium or naphthothiazolium units, respectively. They display no fluorescence due to their electron-withdrawing acceptor structures of cyanine dyes. Upon effective reduction of 3-quinolinium units of probes **A** and **B** by NAD(P)H to electron-donating 1-methyl-1,4-dihydroquinoline units, the probe fluorescence turns on at 572 nm and 586 nm, respectively, with new absorption features at 533 nm and 535 nm, respectively, due to NAD(P)H-activated production of new donor-π-acceptor cyanine platforms. Probe **A** displays a Stokes shift of 39 nm and displays excellent capability for detecting NAD(P)H, with a detection limit of 0.08 μM. Similarly, Probe **B** shows a Stokes shift of 51 nm and has a high sensitivity for determining NAD(P)H, with a detection limit of 0.54 μM. Probe **A** has been effectively used to quantify NAD(P)H levels in live cells during glycolysis when glucose, lactate, and pyruvate are present. It has also been used to assess NAD(P)H levels in $CoCl_2$-induced hypoxic conditions and after exposure to the cancer drugs cisplatin, camptothecin, and gemcitabine. Moreover, probe **A** has been applied to visualize NAD(P)H in first-instar larvae of *D. melanogaster*. Additionally, A549 cancer cell's NAD(P)H levels increase under hypoxic conditions and upon exposure to cancer drugs, including cisplatin, camptothecin, and gemcitabine. Therefore, probe **A** offers unique advantageous features for concurrent visualization of NAD(P)H in living cells, including good sensitivity, exceptional selectivity, speedy responses, simple operations, and spatiotemporal resolution. Moreover, these probes offer a proficient solution to the problem of fluorescence quenching occurring at high NADH concentrations.[24, 26] Unlike cyanine-based fluorescent probes that demonstrate enhanced fluorescence at low NADH concentrations but encounter significant fluorescence quenching as NADH levels rise,[24, 26] the novel probes successfully circumvent this drawback.

EXPERIMENTAL SECTION

Please see supporting documentation for details.

RESULTS AND DISCUSSION

Synthetic methodology

To achieve the primary objective of developing highly sensitive probes for detecting NADH through the integration of a quinolinium-sensing moiety into cyanine dyes, a unique acceptor-π-acceptor platform with weak fluorescence was created using a simple chemical condensation reaction. Starting materials 3-quinolinecarboxaldehyde (**2**) and either 2,3-dimethylbenzo[d]thiazol-3-ium iodide (**1**) or 2,3-dimethylnaphtho[1,2-d]thiazol-3-ium iodide (**4**) was used for the aforementioned condensation reaction. Key intermediates **3** and **5** were formed as a result, and the quinoline moieties of these intermediates were methylated

as depicted in Scheme 2.[20] Two highly sensitive probes were successfully developed and synthesized using this approach, which demonstrated excellent sensitivity and specificity in detecting NAD(P)H. The probes and intermediates were analyzed by NMR and mass spectrometries (Figures S1-S8).

Optical study for NADH sensing

The electronic structure of a molecule determines its optical properties, and π-conjugation plays a key role in defining this structure. When a molecule has alternating single and double bonds, π-electrons can be delocalized across multiple atoms in the molecule, leading to π-conjugation.[20] The extent of π-conjugation within a molecule is critical in revealing its optical properties because it affects the amount of energy required for light absorption. Molecules with a higher degree of π-conjugation have lower energy requirements for light absorption, resulting in longer absorption wavelengths.

In the absence of NADH or, probe **A** exhibits an absorption at 370 nm and probe **B** absorbs at 400 nm due to its enhanced π-conjugation with an additional fused phenyl moiety, as depicted in Figure 1. Upon increasing NADH concentrations, both probes experience significant enhancements in absorption at 533 nm and 535 nm, correspondingly, accompanied by decreases in the absorptions at 370 and 400 nm for probes **A** and **B**, correspondingly. This change in absorption is due to the addition of a hydride from NADH to probes **A** and **B**, resulting in the production of **AH** and **BH** respectively, Scheme 2. This formation results in a rupture in the conjugation within the quinoline sections of the probes, which result in new peaks at 533 nm and 535 nm for **AH** and **BH**, correspondingly (Figure 1).

When NADH is not present, probes **A** and **B** display exceptionally weak fluorescence peaks at 566 nm and 584 nm, respectively, due to the acceptor-π-acceptor fluorophore structures present in their chemical makeup. These structures act as electron acceptors, thereby limiting the extent of π-conjugation and increasing the energy required for the molecule to absorb light. Consequently, the absorption peaks of these probes are shifted towards shorter wavelengths, resulting in weak fluorescence as shown in Figure 2. The restricted internal charge transfer within the two-acceptor molecule is responsible for this weak fluorescence.

Probes **A** and **B** exhibit remarkable sensitivity to NADH, as evidenced by the substantial increase in fluorescence at 572 nm and 586 nm, respectively, upon increasing the NADH concentration from 0 μM to 5 μM. This fluorescence increase is accompanied by a slight red shift. Probes **A** and **B** respond quickly to changes in NADH concentration within a 6-min response time Figure 3, and demonstrate remarkable sensitivity, with detection limits of 0.085 μM and 0.54 μM, respectively (Figure S11). The mechanism responsible for this rapid response arises from the NADH-facilitated reduction of the electron-withdrawing 3-quinolinium acceptors to electron-donating 1,4-dihydroquinoline donors because the reaction products of the probes with NADH were established by electrospray MS spectrometry (Figures S9 for **AH** and S10 for **BH**). This reduction produces well-defined donor-π-acceptor cyanine dyes that are highly fluorescent and offer sensitive detection of NADH (Figure 2).

Probes **A** and **B** demonstrate an impressive level of selectivity for NAD(P)H in comparison to a diverse range of other analytes. This includes cations, such as Co^{2+}, $Fe^{3+,}$ Na^{+}, K^{+}, and Ca^{2+}, anions like Cl^{-}, NO_3^{-}, NO_2^{-}, and SO_4^{2-}, as well as biothiols, such as glutathione and cysteine, amino acids like lysine, methionine and glycine and carbohydrates, such as glucose, ribose, fructose, galactose, lactate, and pyruvate (Figures S12 and S13). This high level of selectivity is significant for the accurate detection and quantification of NAD(P)H, an essential coenzyme that exerts a critical role in energy metabolism and numerous other cellular processes. The propensity for these probes to selectively target NAD(P)H while avoiding interference from other analytes enables the sensitive and specific determination of this critical molecule in complex biological samples.

Theoretical calculations

Theoretical calculations were conducted as described in the supporting information. Interestingly, the optimized geometries indicated a twisted arrangement between the two groups connected by the ethylene bridge with dihedral angles of 25.0°, **A**; −0.59°, **AH**; −42.2°, **B**; 23.6°, **BH**, Figure 4 for probe **AH**. This results in interplanar angles between the thiazolium and quinoline moieties of 19.9°, **A**; 1.3°, **AH**; 45.8°, **B**; and 36.6°, **BH**. Based on these results, a planar arrangement of the molecule may not be the reason for the shift in absorption. While probe **AH** is planar, probe **BH** at 36.6° deviates significantly away from planarity. The values for the calculated absorptions for the probes are in good agreement within the suggested limit of 0.25 eV,[27] **A** 366 nm, calc., (370 nm, expt.), **AH** 449 nm (531 nm), **B** 363 nm (400 nm), **BH** 491 nm (545 nm). Interestingly, while for probes **AH** and **BH**, this absorption (see excited state 1 in Tables S5 and S9 for **AH** and **BH**, respectively) consists solely of a HOMO to LUMO single LCAO transition, that for probes **A** and **B** involves more combinations of orbitals, as is evident in Tables S3 and S7. An examination of the orbitals responsible for excited state 1 for probe **A**, Figure S22, reveals that while the HOMO (orbital 83) is essentially delocalized over the entire molecule, the LUMO (84) is localized in the center. For probe **B**, the illustrations in Figure S26 show that the HOMO (96) is not delocalized possible due to the much larger interplanar angle in **B** of 45.8° compared to that in **A** of 25.0°. Here the electron charge shifts from the thiazolium side of the molecule onto the middle and quinoline sections.

The current density drawing shown in Figure 5, representing the transition associated with excited state 1 in all cases, reveals a remarkable trend in electron density shifts among probes **A** and **B**, as well as their hydrogenated derivatives. In probe **A**, the electron density shifts from either end of the molecule to the left side of the quinolinium moiety. In probe **B**, electron density shifts from the aromatic rings to the sulfur atom within the napthothiazole moiety, as well as shifting towards the ethene group. The addition of a hydride to the probes results in a disruption in the conjugation within the quinoline moiety and for probes **AH** and **BH**, the electron density seems to move away from the carbon atom where the hydride coordinated, shifting towards both the sulfur atom within the benzothiazole moiety, and the nitrogen atom in the quinolinium moiety. This difference in the origin of the transitions is responsible for the change in absorption and thus fluorescence in the probes.

Photostability of the probes

Photostability is a critical characteristic of fluorophores that refers to their ability to resist photobleaching or loss of fluorescence due to prolonged light exposure. Probes **A** and **B** exhibit remarkable photostability, as evidenced by the minimal fluorescence changes of less than 3% observed after excitation for 2 hours at 572 nm, and 586 nm (Figures S14-S15). This property is essential for applications that require long-term or repeated imaging, as photobleaching can lead to loss of signal and decreased image quality over time. The high photostability of probes **A** and **B** makes them valuable tools for imaging and detection applications that require reliable and long-lasting fluorescence measurements.

pH effect on fluorescence responses of the probes to NADH

In our investigation, we examined the fluorescence response of the probes under varying pH conditions both in the presence and absence of NADH. Notably, the probes displayed minimal sensitivity to pH changes when NADH was absent. However, in the presence of NADH, the probes exhibited fluorescence decreases as the pH decreased from 7.5 to 3.0 (see Figures S16 and S17). Interestingly, this behavior aligns with similar observations made for cyanine-based fluorescent probes utilized for NAD(P)H sensing.[26]

Cytotoxicity of the probes

An MTT assay was utilized to verify the toxicity of the probes, as described previously.[20, 28–31] A549 cells were subjected to either probe **A** or **B**, and the enzymatic reduction of the yellow MTT dye to a purple formazan product in the mitochondria was measured as an indicator of cell viability. The MTT assay shows that cell viability is above 80% under a concentration of 40 μM (Figures S18-S19), indicating that the probes are of low toxicity to the cells. Employing a probe with low cytotoxicity can mitigate potential negative impacts on cells, leading to more precise and dependable experimental outcomes. Moreover, low cytotoxicity can enable longer exposure times or repeated measurements over time, which is crucial for longitudinal studies or monitoring treatment effects.

Sensing of NAD(P)H in live cells

Accurately measuring NAD(P)H levels in live cells is crucial due to the coenzyme's involvement in diverse biological processes including energy metabolism and redox homeostasis. [6–24] For this reason, having access to sensitive and compatible probes is essential. In our study, we selected probe **A**, which is both highly sensitive and photostable, to measure levels of NAD(P)H in living cells. After treating A549 cells with 10 μM of probe **A** for 30 minutes, a moderate level of intracellular fluorescence was observed, which is attributed to the presence of intracellular NAD(P)H. To confirm the selectivity of probe **A** for NADH, the cells were preloaded with 20 μM of NADH in glucose-free DMEM medium for 30 minutes, then incubated with probe **A** in glucose-free DMEM medium for varying durations. A gradual increase in cellular fluorescence intensity was noted over time, indicating high selectivity of the probe to NADH (Figure 6). We extended our fluorescence cellular imaging study to include normal fibroblast cells (Figures S20 and S21). These cells were initially incubated with 10 μM probe **A** in glucose-free DMEM medium, followed by incubation with or without 20 μM NADH in the same medium. Over time, we observed a

progressive increase in cellular fluorescence intensity, which reached a stable level within 30 minutes (Figure S20). Interestingly, in the control experiment, we observed that the normal fibroblast cells exhibited a slightly lower NAD(P) level compared to A549 cancer cells (Figure S20).

Glycolysis transforms glucose into pyruvate and results in two molecules of both ATP and NADH per glucose molecule.[32] NADH is a vital coenzyme for several metabolic processes, including cellular respiration and energy production. The NADH molecules generated during glycolysis can be devoted in the electron transport chain found in mitochondria to manufacture more ATP through oxidative phosphorylation.[32] Glucose and NADH levels in live cells are closely linked, where the availability of glucose in the extracellular environment and the cell's ability to absorb and process glucose can affect the rate of glycolysis and NADH production.[32] To demonstrate the possibility of monitoring NADH levels in the presence of extracellular glucose, we utilized probe **A**. We pretreated A549 cells with varying glucose concentrations, alternating from 0 to 20 mM, for 30 minutes, followed by further incubation with 10 μM probe **A** for 30 minutes. An increase in glucose concentration in the cell culture DMEM medium resulted in a corresponding increase in cellular fluorescence intensity, indicating the capacity of the probe to monitor NADH levels during glycolysis (Figure 7). We also conducted the same fluorescence cellular imaging on normal fibroblast cells using probe **A**. After an initial 30-minute incubation with the probe, the cells were further incubated with varying glucose concentrations (0, 5, 10, and 20 mM) in glucose-free DMEM medium (Figure S21). We observed that the cellular fluorescence intensity increased with higher glucose concentrations, indicating the production of NADH in the presence of glucose. This increase in NADH levels can be attributed to the metabolic processes within the cells (Figure S21). Glucose serves as an important energy source for cellular respiration, and its metabolism through glycolysis leads to the generation of NADH. Consequently, higher glucose concentrations in the cell media provide more substrate for glycolysis, resulting in an elevated production of NADH. The elevated NADH levels, in turn, contribute to the increased fluorescence intensity of the probe (Figure S20 and S21). This sensitivity of the probe to changes in NADH concentration enables the detection and visualization of NADH dynamics in live cells.

It is critical to monitor NAD(P)H levels in mitochondria since this cofactor is involved in numerous metabolic processes, including ATP production through oxidative phosphorylation in the mitochondrion.[33] Thus, changes in NAD(P)H levels in mitochondria provide valuable insightful information on the cell's energy status and mitochondrial health. Several diseases, including neurodegenerative disorders, cardiovascular diseases, and cancer, have been associated with variations in the amount of NAD(P)H in mitochondria.[34] For instance, decreased levels of NAD(P)H in mitochondria have been observed in Alzheimer's and Parkinson's disease, indicating that mitochondrial malfunction may contribute to the formation of these diseases.[34–36] Moreover, elevated NAD(P)H levels have been associated with specific cancer types, indicating that mitochondrial metabolism may be altered in cancer cells.[36] To confirm that probe **A** could selectively target mitochondria through electrostatic interactions, a co-incubation experiment was conducted by combining probe **A** with an IR-780 cyanine dye that targets mitochondria in A549 cells. The strong

Pearson correlation coefficient of 0.92 between IR-780 and probe **A** confirmed that probe **A** selectively stains mitochondria (Figure 8). This result provides strong evidence that the positive charges of probe **A** effectively interacted with the negative potential of mitochondria, enabling the specificity of the probe to the mitochondria.

NADH plays a crucial role as a cofactor in glycolysis, being produced during the transformation of glyceraldehyde-3-phosphate into 1,3-bisphosphoglycerate, and is closely related to the generation of lactate and pyruvate.[37] In hypoxic conditions, pyruvate is transformed into lactate, leading to the regeneration of NAD^+ from NADH, which allows glycolysis to continue and sustain ATP production.[37, 38] On the other hand, under aerobic conditions, pyruvate is transferred to the mitochondria where it experiences further metabolism in the TCA cycle, generating NADH that is employed by the electron transport chain to create ATP. [37] The monitoring of NADH levels during glycolysis in cancer cells is important to understand their metabolic state, and the presence of lactate and pyruvate provides insight into the control of cellular metabolism and the progression of cancer. Our investigation revealed that treating A549 cells with 10 mM lactate led to an increase in cellular fluorescence intensity, while treatment with 5 mM pyruvate resulted in a decrease. Cells treated with a mixture of 5 mM pyruvate and 10 mM lactate showed higher cellular fluorescence intensity than control cells without treatment (Figure 9).

Under hypoxic conditions, cells experience a shortage of oxygen, leading to a reduction in the effectiveness of the electron transport chain that relies on oxygen to produce ATP.[37] As a result, cells rely more heavily on glycolysis, a process that generates ATP without requiring oxygen, resulting in the accumulation of NADH and NADPH.[39] Furthermore, the conversion of NAD^+ to NADH, which is necessary for the conversion of pyruvate to lactate through the activity of lactate dehydrogenase, further reduces the levels of NAD^+. This reduction in NAD^+ levels contributes to the ratio increase of NADH to NAD^+, which is a crucial parameter for regulating many cellular metabolic pathways, including signaling pathways and gene expression.[40] Monitoring NAD(P)H levels is essential for understanding the metabolic state of cells and their response to stress. We employed cobalt chloride ($CoCl_2$) to trigger hypoxia and used probe **A** to determine NAD(P)H levels in A549 cells. $CoCl_2$ is a hypoxia-mimicking agent that stabilizes the HIF-1α subunit by inhibiting its prolyl hydroxylation, which triggers its degradation under normoxic conditions.[41] HIF-1α is a transcription factor activated under low-oxygen circumstances, and its stabilization can induce the upregulation of downstream target genes involved in adaptation to hypoxia, such as those involved in angiogenesis, erythropoiesis, and glycolysis.[42, 43] $CoCl_2$ has been widely used as a tool to study cellular responses to hypoxia because of its ease of use and reproducibility.[44] It has been reported to provoke hypoxia-like responses in various cell types, including cancer cells, neuronal cells, and endothelial cells.[44–46] Our results using probe **A** showed that the intensity of cellular fluorescence increased significantly with increasing doses of $CoCl_2$, indicating that the probe could be exploited to assess alterations in NAD(P)H levels under hypoxic conditions (Figure 10). This finding highlights the probe's potential as a useful tool for monitoring cellular responses to hypoxia and further exploring the underlying mechanisms of cellular adaptation to stress.

The drug cisplatin is frequently used in chemotherapy to damage the DNA of rapidly dividing cancer cells.[47–49] Our findings reveal that increasing doses of cisplatin lead to increases in NAD(P)H levels in A549 cells (Figure 11). One potential explanation for this observation is that the DNA damage initiated by cisplatin stimulates the poly(ADP-ribose) polymerase (PARP) pathway, which utilizes NAD^+ to synthesize poly(ADP-ribose) (PAR) chains on damaged DNA. PARylation can facilitate the mobilization of DNA repair factors to the damaged site and aid in the repair process.[47–49] However, excessive PARylation can deplete NAD^+, which can negatively affect cellular metabolism and energy production. Cells can replenish NAD^+ via the salvage pathway, where nicotinamide is converted to NAD^+ by the enzyme nicotinamide phosphoribosyltransferase (NAMPT). NAMPT is upregulated under stress conditions to facilitate this process.[50] Another possible mechanism for cisplatin-induced NAD(P)H level increases can be the stimulation of the Nrf2 pathway, a crucial regulator of antioxidant defense and stress response genes. Nrf2 can be activated by various stress stimuli, including oxidative stress, and can enhance the expression of genes that contribute to NAD(P)H production, such as glucose-6-phosphate dehydrogenase (G6PD), an enzyme that is rate-limiting in the pentose phosphate pathway (PPP).[51] The PPP is an alternative pathway for glucose metabolism that generates NAD(P)H, a reducing equivalent that is critical for antioxidant defense and lipid synthesis.[52] Thus, the increase in NAD(P)H levels in A549 cells administered with increasing doses of cisplatin may result from the activation of the PARP and Nrf2 pathways,[53] which could lead to NAD^+ consumption and NADPH production, respectively. These mechanisms may represent adaptive responses of cancer cells to cope with cisplatin-induced stress and may contribute towards the development of cisplatin resistance.[53] Further understanding the molecular mechanisms that underlie cisplatin-induced changes in NAD(P)H levels can offer insights into the metabolic weaknesses of cancer cells and facilitate the development of novel strategies to circumvent drug resistance.

The antimetabolite chemotherapy drug, gemcitabine, has been used to treat cancer.[54–57] Antimetabolites disrupt the process of DNA replication,[58] which is crucial for cell division. In addition to its inhibitory effects on DNA synthesis, gemcitabine also affects cellular metabolism and energy production, which may lead to its antitumor effects.[54–57] When administered at various doses, gemcitabine results in an increase in the NAD(P)H levels in A549 cancer cells (Figure 12). Numerous metabolic pathways, involving glycolysis and the citric acid cycle, are dependent on these coenzymes. This mechanism by which the increase in NAD(P)H levels is caused by gemcitabine remains to be discovered. It is theorized that a decline in the amount of deoxynucleotide molecules, resulting from the action of gemcitabine on ribonucleotise, correlates with an increase in NAD(P)H. It is therefore likely that the increase in NAD(P)H levels by adding gemcitabine is the reason for its antitumor capabilities and there may be changes to normal cellular metabolism and energy production which result in apoptosis.[54–57] Further research is required to fully clarify these points.

Camptothecin is a type of chemotherapy medication utilized for treating various cancers, including A549 lung cancer.[59–61] It functions by inhibiting topoisomerase I, inducing cell cycle arrest and apoptosis in cancerous cells and affecting cellular metabolism and energy production.[59–61] Administering camptothecin to A549 cancer cells causes increased levels of NAD(P)H (Figure 13). The specific mechanisms by which camptothecin increases

NAD(P)H levels are not entirely clear. Camptothecin treatment of A549 cells causes DNA damage, activating DNA repair mechanisms. [59–61] This activation could result in an increased demand for NAD+ since the enzyme poly(ADP-ribose) polymerase (PARP), involved in DNA repair, consumes it. As a result, NADH and NADPH levels increase, impacting cellular processes, energy production, and ultimately contributing to antitumor effects and apoptosis.[62]

Vancomycin functions as an antibiotic by binding to the terminal D-Ala-D-Ala residues, disrupting the synthesis of the bacterial cell wall.[63–65] However, it also has non-antibiotic effects, such as inhibiting the mitochondrial complex I enzyme that exerts a critical role in energy production and cellular respiration.[66] At a concentration of 5 μM, vancomycin may bind to and inhibit complex I in A549 cancer cells, causing a reduction in electron transport chain activity and ATP production (Figure 14). This decline in ATP production can trigger an increase in NADH levels, as the electron transport chain produces NADH when there is a decrease in electron transport. However, at higher concentrations of vancomycin with 10 μM and 20 μM, the drug's antibiotic effects may take precedence, causing cell death and reducing metabolic activity. [63–65] This reduction in metabolic activity can result in a decline in NADH levels, as there is less electron transport and hence less NADH production (Figure 14). It is also possible that the effects of vancomycin on NADH levels in A549 cancer cells may depend on other factors such as the cell's energy demands, oxidative stress levels, and mitochondrial function. Additional research is required to fully delineate the underlying mechanisms.

Sensing of NAD(P)H in first-instar larvae of *D. melanogaster*

NAD(P)H is one of the major components for energy production, cellular metabolism, and redox signaling, underscoring the need to monitor its levels in developing organisms. Herein, we evaluated the effectiveness of probe **A** in detecting NAD(P)H levels in just-hatched first-instar larvae of the model organism *D. melanogaster*. To ensure consistency in NAD(P)H levels across the larvae, we let them hatch without feeding by placing fruit fly eggs on a moist paper towel. After incubating the larvae with 10 μM probe **A** in pH 7.4 PBS buffer for 30 minutes, we observed moderate fluorescence intensity within the fruit fly larvae, indicating lower levels of NAD(P)H owing to the lack of food after hatching (Figure 15). In contrast, fruit fly larvae that were not washed off the egg-lay plates containing sugar showed a much stronger fluorescence intensity (Figure 16), indicating higher levels of NAD(P)H within the larvae because they started feeding after hatching. To further investigate variations in NADH levels, we incubated the starvation-hatched larvae with different concentrations of NADH for 15 minutes, washed them with pH 7.4 PBS buffer three times, and then incubated these NADH-fed fruit fly larvae with 10 μM probe **A** for 30 minutes. This produced a considerable increase of the fluorescence intensity for fruit fly larvae with increasing NADH concentrations, highlighting the potential of probe **A** in investigating NAD(P)H dynamics in developing organisms and providing valuable insights into the regulation of cellular metabolism during development.

CONCLUSIONS

In summary, we have developed highly sensitive cyanine dyes, probes **A** and **B**, by linking benzothiazolium and 2,3-dimethylnaphtho[1,2-d]thiazol-3-ium units to 3-quinolinium through a vinyl bond. These probes detect NAD(P)H levels rapidly and sensitively, as indicated by increases in new fluorescence emissions upon NAD(P)H reaction, demonstrating the reduction of their electron-deficient 3-quinolinium units. Probe **A** was also utilized to monitor NADH levels in live cells during glycolysis, hypoxic conditions induced by $CoCl_2$ treatment, and after exposure to cancer drugs, including cisplatin, camptothecin, and gemcitabine. Furthermore, probe **A** enabled us to visualize NADH changes in *D. melanogaster* first-instar larvae. Overall, our results suggest that probe **A** holds great utility for biological applications, particularly for the sensing of NAD(P)H in cancer cells and for monitoring metabolic processes.

Supplementary Material

Refer to Web version on PubMed Central for supplementary material.

ACKNOWLEDGMENTS

The research study was sponsored by the National Institute of General Medical Sciences, National Institutes of Health, through Award Numbers 2R15GM114751 and R15GM114751 for H.Y. Liu, and R15 GM146206-01 for H.Y. Liu and R. L. Luck. We would also like to express our gratitude to the National Science Foundation for their financial assistance under award number 2117318. This funding enabled us to acquire a new NMR spectrometer to characterize chemical structures of the fluorescent probes, with H. Liu as one of the recipients of the grant. We performed computational calculations for the fluorescent probes using a high-performance computing infrastructure located at Michigan Technological University. We acknowledge the support of these organizations in making this research possible.

REFERENCES:

(1). Moller IM; Rasmusson AG The role of NADP in the mitochondrial matrix. Trends Plant Sci. 1998, 3 (1), 21–27.

(2). Kulikova VA; Gromyko DV; Nikiforov AA The Regulatory Role of NAD in Human and Animal Cells. Biochem. (Mosc.) 2018, 83 (7), 800–812.

(3). Walker MA; Tian R. NAD(H) in mitochondrial energy transduction: implications for health and disease. Curr. Opin. Physiol 2018, 3, 101–109. [PubMed: 32258851]

(4). Somogyi A; Horvai G; Csala M; Toth B. Analytical Approaches for the Quantitation of Redox-active Pyridine Dinucleotides in Biological Matrices. Period. Polytech-Chem 2016, 60 (4), 218–230.

(5). Xiao WS; Wang RS; Handy DE; Loscalzo J. NAD(H) and NADP(H) Redox Couples and Cellular Energy Metabolism. Antioxid. Redox Signal 2018, 28 (3), 251–272. [PubMed: 28648096]

(6). Sun PJ; Zhang HX; Sun YQ; Liu J. The recent development of fluorescent probes for the detection of NADH and NADPH in living cells and in vivo. Spectrochim. Acta A-Mol. Biomol. Spectrosc 2021, 245, 118919. [PubMed: 32977107]

(7). Noguchi T; Dawn A; Yoshihara D; Tsuchiya Y; Yamamoto T; Shinkai S. Selective Detection of NADPH among Four Pyridine-Nucleotide Cofactors by a Fluorescent Probe Based on Aggregation-Induced Emission. Macromol. Rapid Commun 2013, 34 (9), 779–784. [PubMed: 23495077]

(8). Santra M; Sarkar S; Jun YW; Reo YJ; Ahn KH Dual probing of redox species, NAD(P)H and HOCl, with a benzo a phenoxazine based far red-emitting dye. Tetrahedron Lett. 2018, 59 (33), 3210–3213.

(9). Zhao YH; Wei KY; Kong FP; Gao XN; Xu KH; Tang B. Dicyanoisophorone-Based Near-Infrared-Emission Fluorescent Probe for Detecting NAD(P)H in Living Cells and in Vivo. Anal. Chem 2019, 91 (2), 1368–1374. [PubMed: 30525465]

(10). Jiang L; Lei X; Wang KJ; Zhang ZJ; Wang F; Lu S; Chen XQ Colorimetric and fluorometric detection of NADPH using imidazolium functionalized polydiacetylenes with high sensitivity and selectivity. Dyes Pigm. 2020, 183, 108740.

(11). Tian Y; Jiang WL; Wang WX; Mao GJ; Li YF; Li CY NAD(P)H-triggered probe for dual-modal imaging during energy metabolism and novel strategy of enhanced photothermal therapy in tumor. Biomaterials 2021, 271, 120736. [PubMed: 33662745]

(12). Wang L; Zhang JY; Kim B; Peng JJ; Berry SN; Ni Y; Su DD; Lee J; Yuan L; Chang YT Boronic Acid: A Bio-Inspired Strategy To Increase the Sensitivity and Selectivity of Fluorescent NADH Probe. J. Am. Chem. Soc 2016, 138 (33), 10394–10397. [PubMed: 27500425]

(13). Podder A; Koo S; Lee J; Mun S; Khatun S; Kang HG; Bhuniya S; Kim JS A rhodamine based fluorescent probe validates substrate and cellular hypoxia specific NADH expression. Chem. Commun 2019, 55 (4), 537–540.

(14). Podder A; Murali VP; Deepika S; Dhamija A; Biswas S; Maiti KK; Bhuniya S. NADH-Activated Dual-Channel Fluorescent Probes for Multicolor Labeling of Live Cells and Tumor Mimic Spheroids. Anal. Chem 2020, 92 (18), 12356–12362. [PubMed: 32814423]

(15). Podder A; Thirumalaivasan N; Chao YK; Kukutla P; Wu SP; Bhuniya S. Two-photon active fluorescent indicator for detecting NADH dynamics in live cells and tumor tissue. Sens. Actuators B Chem 2020, 324, 128637.

(16). Sharma H; Tan NK; Trinh N; Yeo JH; New EJ; Pfeffer FM A fluorescent naphthalimide NADH mimic for continuous and reversible sensing of cellular redox state. Chem. Commun 2020, 56 (15), 2240–2243.

(17). Hong SN; Pawel GT; Pei RJ; Lu Y. Recent progress in developing fluorescent probes for imaging cell metabolites. Biomed. Mater 2021, 16 (4), 044108.

(18). Li MZ; Liu C; Zhang WJ; Xu LF; Yang MM; Chen ZL; Wang XX; Pu LL; Liu WL; Zeng XS; Wang TH An NADH-selective and sensitive fluorescence probe to evaluate living cell hypoxic stress. J Mater. Chem. B 2021, 9 (46), 9547–9552. [PubMed: 34761793]

(19). Park SY; Yoon SA; Cha YJ; Lee MH Recent advances in fluorescent probes for cellular antioxidants: Detection of NADH, hNQO1, H2S, and other redox biomolecules. Coord. Chem. Rev 2021, 428, 213613.

(20). Zhang YB; Arachchige DL; Olowolagba A; Luck RL; Liu HY Near-infrared fluorescent probe based on rhodamine derivative for detection of NADH in live cells. Methods 2022, 204, 22–28. [PubMed: 35381337]

(21). Wang Q; Zhu YZ; Chen DB; Ou JL; Chen M; Feng Y; Wang WB; Meng XM A dual-salt fluorescent probe for specific recognition of mitochondrial NADH and potential cancer diagnosis. Talanta 2023, 257, 124393. [PubMed: 36858015]

(22). Joo JH; Youn D; Park SY; Shin DS; Lee MH Mitochondria-targetable red-emitting probe for real-time fluorescence monitoring of NAD(P)H in live cells. Dyes Pigments 2019, 170, 107561.

(23). Joo JH; Won M; Park SY; Park K; Shin DS; Kim JS; Lee MH A dicyanocoumarin-fused quinolinium based probe for NAD(P)H and its use for detecting glycolysis and hypoxia in living cells and tumor spheroids. Sens. Actuators B Chem 2020, 320, 128360.

(24). Fomin MA; Dmitriev RI; Jenkins J; Papkovsky DB; Heindl D; Konig B. Two-Acceptor Cyanine-Based Fluorescent Indicator for NAD(P)H in Tumor Cell Models. ACS Sens. 2016, 1 (6), 702–709.

(25). Ouyang J; Sun LH; Zeng F; Wu SZ Biomarker-activatable probes based on smart AIEgens for fluorescence and optoacoustic imaging. Coord. Chem. Rev 2022, 458, 214438.

(26). Dwivedi SK; Arachchige DL; Olowolagba A; Mahmoud M; Cunnien J; Tucker DR; Fritz D; Werner T; Luck RL; Liu HY Thiophene-based organic dye with large Stokes shift and deep red emission for live cell NAD(P)H detection under varying chemical stimuli. J. Mater. Chem. B 2023, 11 (27), 6296–6307. [PubMed: 37249441]

(27). Jacquemin D; Wathelet V; Perpète EA; Adamo C. Extensive TD-DFT Benchmark: Singlet-Excited States of Organic Molecules. J. Chem. Theory Comput 2009, 5 (9), 2420–2435. [PubMed: 26616623]

(28). Wang JB; Xia S; Bi JH; Fang MX; Mazi WF; Zhang YB; Conner N; Luo FT; Lu HP; Liu HY Ratiometric Near-Infrared Fluorescent Probes Based On Through Bond Energy Transfer and pi-Conjugation Modulation between Tetraphenylethene and Hemicyanine Moieties for Sensitive Detection of pH Changes in Live Cells. Bioconjugate Chem. 2018, 29 (4), 1406–1418.

(29). Zhang YB; Xia S; Mikesell L; Whisman N; Fang MX; Steenwinkel TE; Chen K; Luck RL; Werner T; Liu HY Near-Infrared Hybrid Rhodol Dyes with Spiropyran Switches for Sensitive Ratiometric Sensing of pH Changes in Mitochondria and Drosophila melanogaster First-Instar Larvae. ACS Appl. Bio Mater 2019, 2 (11), 4986–4997.

(30). Xia SA; Wang JB; Zhang YB; Whisman N; Bi JH; Steenwinkel TE; Wan SL; Medford J; Tajiri M; Luck RL; Werner. T.; Liu, H.Y. Ratiometric fluorescent probes based on through-bond energy transfer of cyanine donors to near-infrared hemicyanine acceptors for mitochondrial pH detection and monitoring of mitophagy. J. Mater. Chem. B 2020, 8 (8), 1603–1615. [PubMed: 32055810]

(31). Dwivedi SK; Arachchige DL; Vohs T; Tang J; Usimaki K; Olowoagba AM; Fritz DR; Luck RL; Werner T. and Liu HY Near-infrared rhodol dyes bearing salicylaldehyde moieties for ratiometric pH sensing in live cells during mitophagy and under hypoxia conditions. J. Mater. Chem. B 2023, 11, 2852–2861. [PubMed: 36808460]

(32). Circu ML; Maloney RE; Aw TY Low glucose stress decreases cellular NADH and mitochondrial ATP in colonic epithelial cancer cells: Influence of mitochondrial substrates. Chemico-Biological Interactions 2017, 264, 16–24. [PubMed: 28087461]

(33). Cairns CB; Walther J; Harken AH; Banerjee A. Mitochondrial oxidative phosphorylation thermodynamic efficiencies reflect physiological organ roles. Am. J. Physiol. Regul. Integr. Comp. Physiol 1998, 274 (5), R1376–R1383.

(34). Bhatti JS; Bhatti GK; Reddy PH Mitochondrial dysfunction and oxidative stress in metabolic disorders - A step towards mitochondria based therapeutic strategies. Biochim. Biophys. Acta. Mo.l Basis. Dis 2017, 1863 (5), 1066–1077.

(35). Ortiz JMP; Swerdlow RH Mitochondrial dysfunction in Alzheimer's disease: Role in pathogenesis and novel therapeutic opportunities. Br. J. Pharmacol 2019, 176 (18), 3489–3507. [PubMed: 30675901]

(36). Amjad S; Nisar S; Bhat AA; Shah AR; Frenneaux MP; Fakhro K; Haris M; Reddy R; Patay Z; Baur J; Bagga R. Role of NAD(+) in regulating cellular and metabolic signaling pathways. Mol. Metab 2021, 49. 101195.

(37). Voige WH; Lamb CE COMPUTER-AIDED-INSTRUCTION IN BIOCHEMISTRY - INTERACTIVE PROGRAM TO HELP STUDENTS UNDERSTAND ANAEROBIC GLYCOLYSIS. Fed. Proc 1979, 38 (3), 804-804.

(38). Luengo A; Li ZQ; Gui DY; Sullivan LB; Zagorulya M; Do BT; Ferreira R; Naamati A; Ali A; Lewis CA; Thomas CJ; Spranger S; Matheson NJ; Heiden MGV Increased demand for NAD(+) relative to ATP drives aerobic glycolysis. Mol. Cell 2021, 81 (4), 691. [PubMed: 33382985]

(39). Xie N; Zhang L; Gao W; Huang CH; Huber PE; Zhou XB; Li CL; Shen GB; Zou BW NAD(+)metabolism: pathophysiologic mechanisms and therapeutic potential. Signal Transduct. Target. Ther 2020, 5 (1), 227. [PubMed: 33028824]

(40). Yang Y; Sauve AA NAD(+) metabolism: Bioenergetics, signaling and manipulation for therapy. Biochim. Biophys. Acta - Proteins Proteom 2016, 1864 (12), 1787–1800.

(41). Di Mattia M; Mauro A; Delle Monache S; Pulcini F; Russo V; Berardinelli P; Citeroni MR; Turriani M; Peserico A; Barboni B. Hypoxia-Mimetic CoCl2 Agent Enhances Pro-Angiogenic Activities in Ovine Amniotic Epithelial Cells-Derived Conditioned Medium. Cells 2022, 11 (3), 461. [PubMed: 35159271]

(42). Quintero M; Mackenzie N; Brennan PA Hypoxia-inducible factor I (HIF-1) in cancer. Ejso 2004, 30 (5), 465–468. [PubMed: 15135470]

(43). Ishikawa H; Xu LL; Sone K; Kobayashi T; Wang GW; Shozu M. Hypoxia Induces Hypoxia-Inducible Factor 1 alpha and Potential HIF-Responsive Gene Expression in Uterine Leiomyoma. Reprod. Sci 2019, 26 (3), 428–435. [PubMed: 29779471]

(44). Wan SL; Vohs T; Steenwinkel TE; White WR; Lara-Ramirez A; Luck RL; Werner T; Tanasova M; Liu HY Near-Infrared Fluorescent Probes with Amine-Incorporated Xanthene Platforms for the Detection of Hypoxia. ACS Appl. Bio Mater 2022, 5 (9), 4294–4300.

(45). Ciafre SA; Niola F; Giorda E; Farace MG; Caporossi D. CoCl2-simulated hypoxia in skeletal muscle cell lines: Role of free radicals in gene up-regulation and induction of apoptosis. Free Radical Res. 2007, 41 (4), 391–401. [PubMed: 17454121]

(46). Kutryb-Zajac B; Kawecka A; Braczko A; Franczak M; Slominska EM; Giovannoni R; Smolenski RT CoCl2-Mimicked Endothelial Cell Hypoxia Induces Nucleotide Depletion and Functional Impairment That Is Reversed by Nucleotide Precursors. Biomedicines 2022, 10 (7), 1540. [PubMed: 35884844]

(47). Hettinga JVE; Konings AWT; Kampinga HH Reduction of cellular cisplatin resistance by hyperthermia - a review. Int. J. Hyperthermia 1997, 13 (5), 439–457. [PubMed: 9354931]

(48). Yao X; Panichpisal K; Kurtzman N; Nugent K. Cisplatin nephrotoxicity: A review. Am. J. Med. Sci 2007, 334 (2), 115–124. [PubMed: 17700201]

(49). Torso ND; Pereira JKN; Visacri MB; Vasconcelos P; Loren P; Saavedra K; Saavedra N; Salazar LA; Moriel P. Dysregulated MicroRNAs as Biomarkers or Therapeutic Targets in Cisplatin-Induced Nephrotoxicity: A Systematic Review. Int. J. Mol. Sci 2021, 22 (23), 12765. [PubMed: 34884570]

(50). Murata MM; Kong XD; Moncada E; Chen YM; Imamura H; Wang P; Berns MW; Yokomori K; Digman MA NAD plus consumption by PARP1 in response to DNA damage triggers metabolic shift critical for damaged cell survival. Mol. Biol. Cell 2019, 30 (20), 2584–2597. [PubMed: 31390283]

(51). Tebay LE; Robertson H; Durant ST; Vitale SR; Penning TM; Dinkova-Kostova AT; Hayes JD Mechanisms of activation of the transcription factor Nrf2 by redox stressors, nutrient cues, and energy status and the pathways through which it attenuates degenerative disease. Free Radical Biol. Med 2015, 88, 108–146. [PubMed: 26122708]

(52). Stincone A; Prigione A; Cramer T; Wamelink MMC; Campbell K; Cheung E; Olin-Sandoval V; Gruning NM; Kruger A; Alam MT Keller, V.O.; Breitenbach, M.; Brindle, K.M.; Rabinowitz, J.D.; Ralser, M. The return of metabolism: biochemistry and physiology of the pentose phosphate pathway. Biol. Rev 2015, 90 (3), 927–963. [PubMed: 25243985]

(53). Chen Q; Peng HX; Dong L; Chen LJ; Ma XB; Peng YP; Dai SJ; Liu Q. Activation of the NRF2-ARE signalling pathway by the Lentinula edodes polysaccharose LNT alleviates ROS-mediated cisplatin nephrotoxicity. Int. Immunopharmacol 2016, 36, 1–8. [PubMed: 27093515]

(54). Dingle BH; Rumble RB; Brouwers MC; Canc Care Ontarios Program, E. The role of gemcitabine in the treatment of cholangiocarcinoma and gallbladder cancer: A systematic review. Can. J. Gastroenterol. Hepatol 2005, 19 (12), 711–716.

(55). Dent S; Messersmith H; Trudeau M. Gemcitabine in the management of metastatic breast cancer: a systematic review. Breast Cancer Res. Treat 2008, 108 (3), 319–331. [PubMed: 17530427]

(56). Silvestris N; Cinieri S; La Torre I; Pezzella G; Numico G; Orlando L; Lorusso V. Role of gemcitabine in metastatic breast cancer patients: A short review. Breast 2008, 17 (3), 220–226. [PubMed: 18037292]

(57). Shelley MD; Jones G; Cleves A; Wilt TJ; Mason MD; Kynaston HG Intravesical gemcitabine therapy for non-muscle invasive bladder cancer (NMIBC): a systematic review. BJU Int. 2012, 109 (4), 496–505. [PubMed: 22313502]

(58). Lansiaux A. Antimetabolites. Bull. Cancer 2011, 98 (11), 1263–1274. DOI: 10.1684/bdc.2011.1476. [PubMed: 22049385]

(59). Sriram D; Yogeeswari P; Thirumurugan R; Bal TR Camptothecin and its analogues: a review on their chemotherapeutic potential. Nat. Prod. Res 2005, 19 (4), 393–412. [PubMed: 15938148]

(60). Legarza K; Yang LX New molecular mechanisms of action of camptothecin-type drugs. Anticancer Res. 2006, 26 (5A), 3301–3305. [PubMed: 17094444]

(61). Li QY; Zu YG; Shi RZ; Yao LP Review Camptothecin: Current Perspectives. Curr. Med. Chem 2006, 13 (17), 2021–2039. [PubMed: 16842195]

(62). Liskova V; Kajsik M; Chovancova B; Roller L; Krizanova O. Camptothecin, triptolide, and apoptosis inducer kit have differential effects on mitochondria in colorectal carcinoma cells. Febs Open Bio 2022, 12 (5), 913–924.

(63). DiMondi VP; Rafferty K. Review of Continuous-Infusion Vancomycin. Ann. Pharmacother 2013, 47 (2), 219–227. [PubMed: 23386074]

(64). Mejias-Trueba M; Alonso-Moreno M; Herrera-Hidalgo L; Gil-Navarro MV Target Attainment and Clinical Efficacy for Vancomycin in Neonates: Systematic Review. Antibiotics. 2021, 10 (4). 347. [PubMed: 33805874]

(65). Selim S. Mechanisms of gram-positive vancomycin resistance (Review). Biomed. Rep 2022, 16 (1), 7. [PubMed: 34938536]

(66). Suarez-Rivero JM; Pastor-Maldonado CJ; Povea-Cabello S; Alvarez-Cordoba M; Villalon-Garcia I; Talaveron-Rey M; Suarez-Carrillo A; Munuera-Cabeza M; Sanchez-Alcazar JA Mitochondria and Antibiotics: For Good or for Evil? Biomolecules 2021, 11 (7), 1050. [PubMed: 34356674]

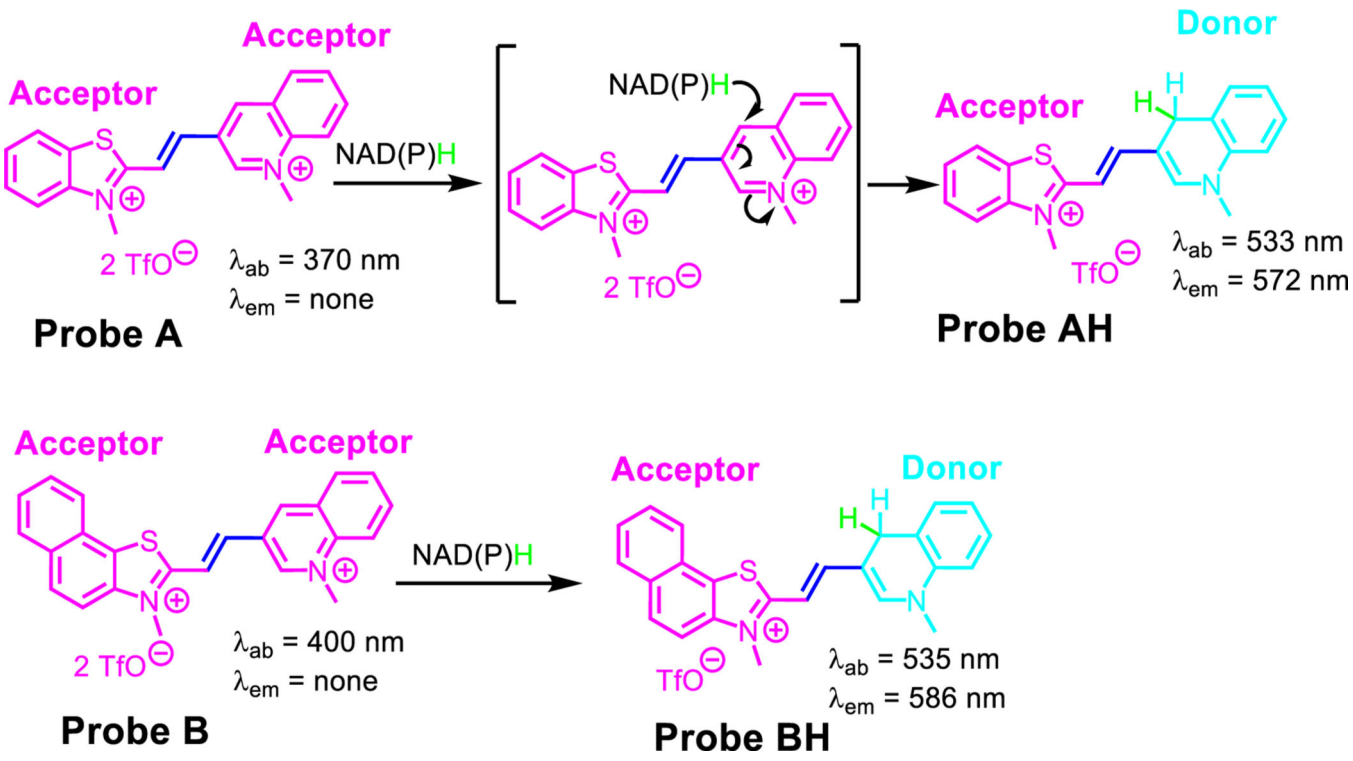

Scheme 1.
NADH reactions with probes **A** and **B**.

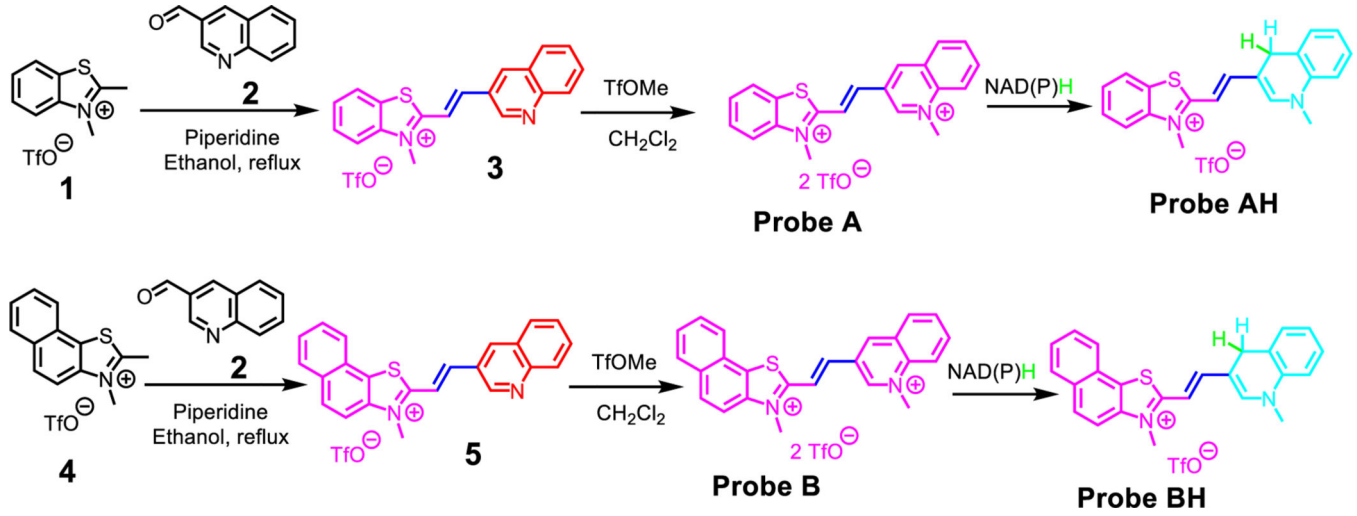

Scheme 2.

Preparative routes to prepare probes **A** and **B**.

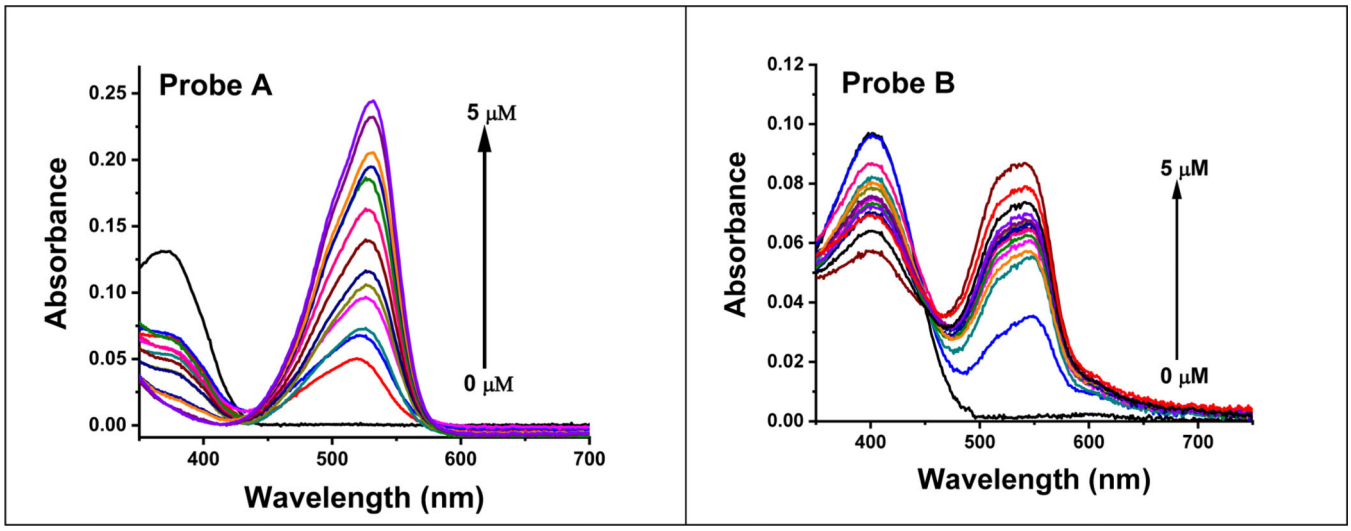

Figure 1.

The absorption spectra of probe **A** (left) and probe **B** (right) at a concentration of 10 μM were recorded without and with changing concentrations of NADH, following a 6-minute incubation of NADH with the probes.

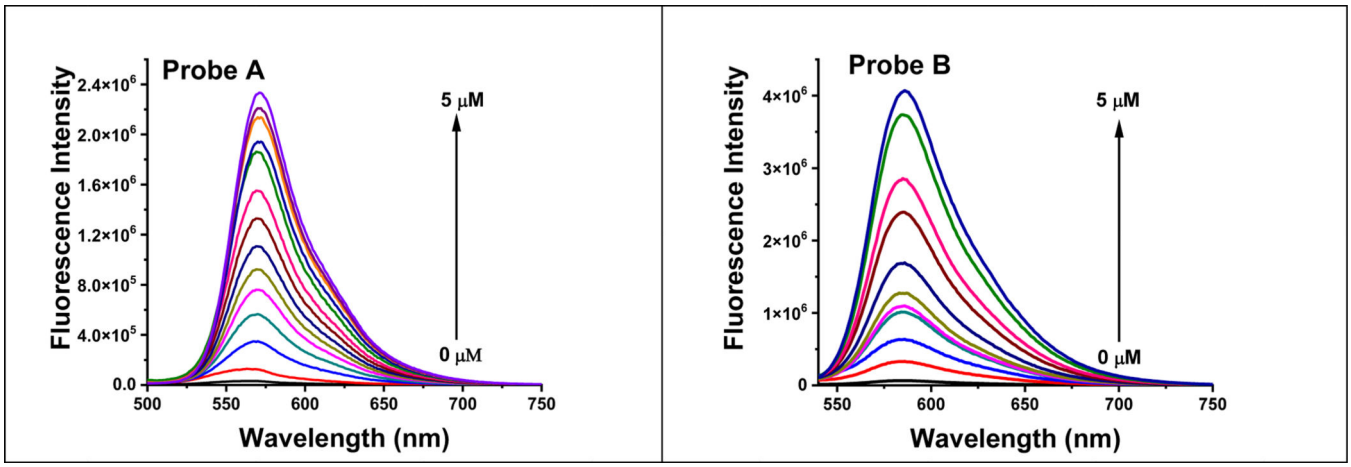

Figure 2.

The fluorescence spectra of probe **A** (left) and probe **B** (right) at a concentration of 10 μM were recorded with varying concentrations of NADH under 520 nm excitation. The probes were incubated with NADH for 6 minutes prior to the measurement.

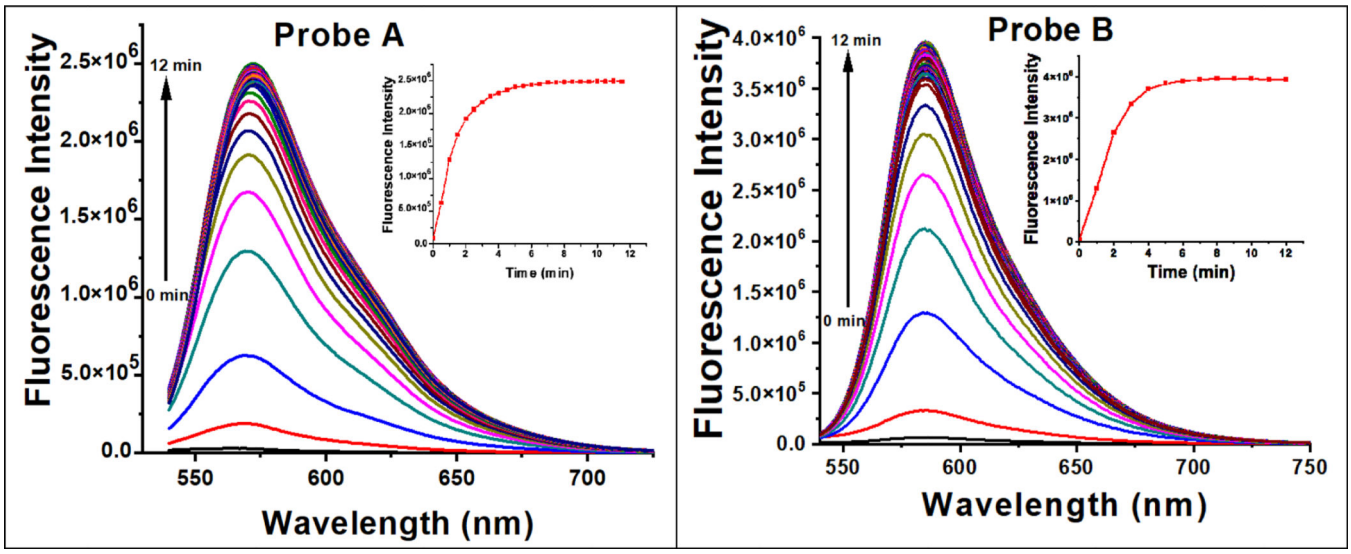

Figure 3.

Luminescence spectra of 10 μM probe **A** (left) and **B** (right) as a function of time with NADH (5 μM) under 520 nm excitation.

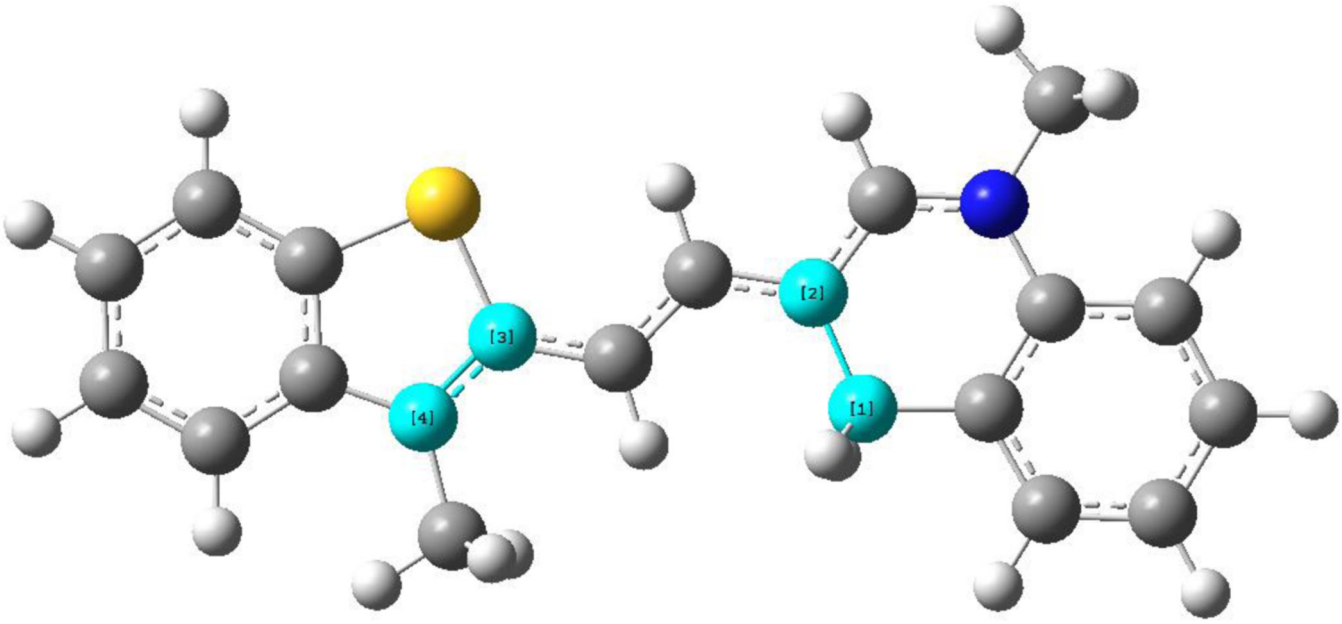

Figure 4.
Atoms used for dihedral angle calculation between bridged groups in probe **AH**.

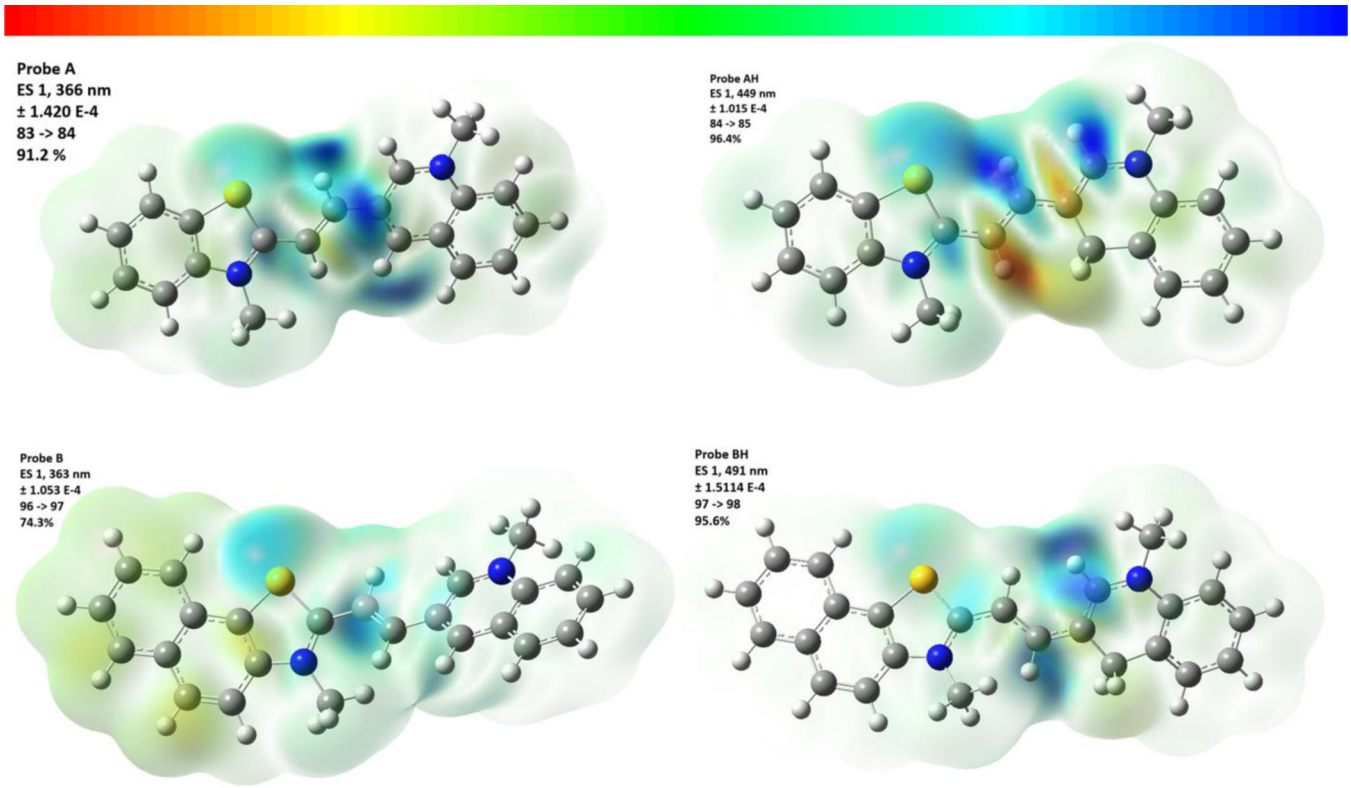

Figure 5.

3D surface illustrations of probes **A**, **AH**, **B**, and **BH** depicting the electron density variance for their primary electron transitions. The top of the figure displays the color scale values. Please refer to the Supplementary Material for diagrams illustrating the molecular orbitals associated with these transitions.

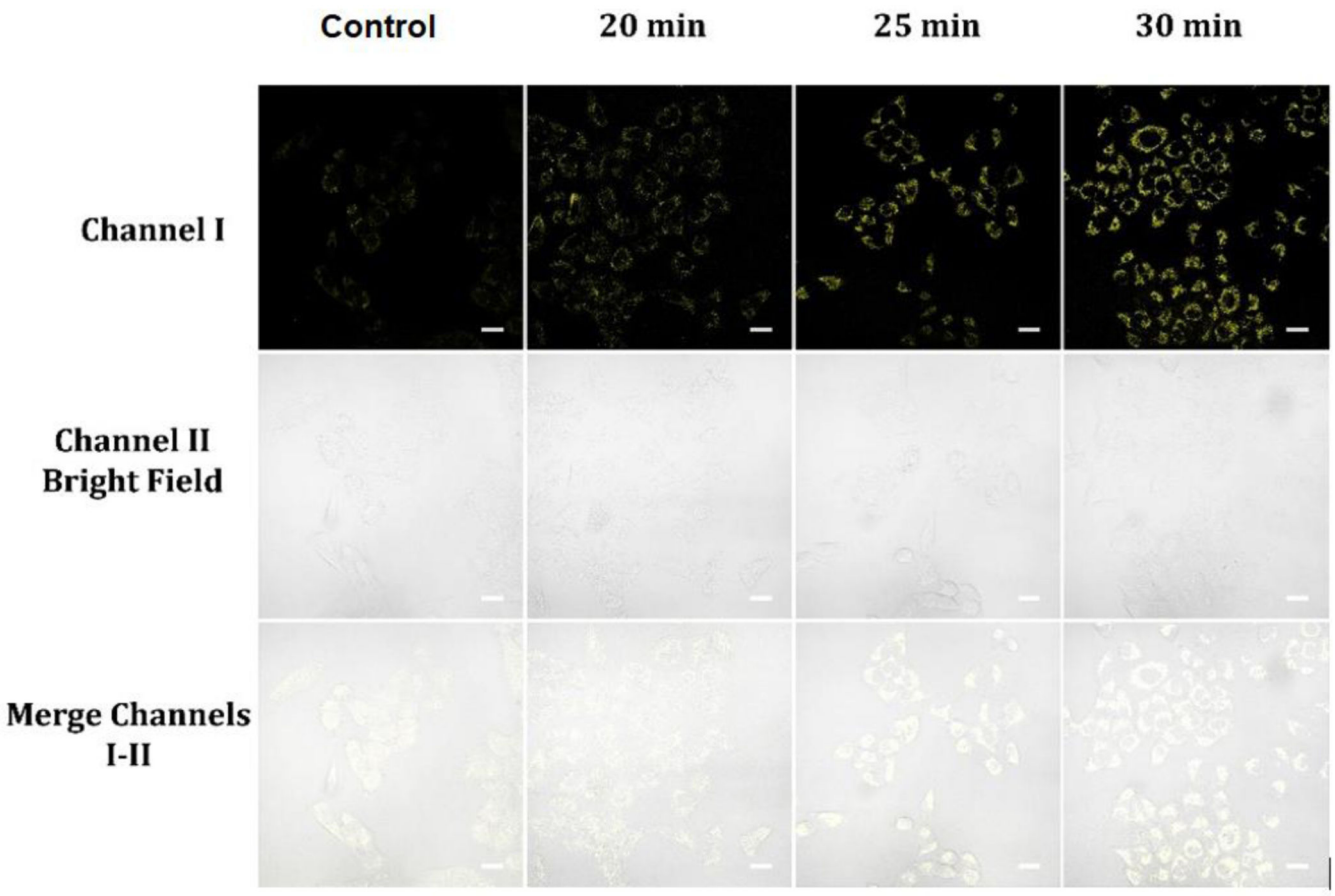

Figure 6.

Cellular luminescence images of A549 cells preloaded with 20 μM NADH in glucose-free DMEM medium for 30 minutes and cultivated with 10 μM probe **A** in glucose-free DMEM medium for varying incubation times, as well as a control image of A549 cells cultivated with 10 μM probe **A** in glucose-free DMEM medium for 30 minutes. Image fluorescence signals were captured between 550 to 650 nm upon 488 nm excitation for both sets of images.

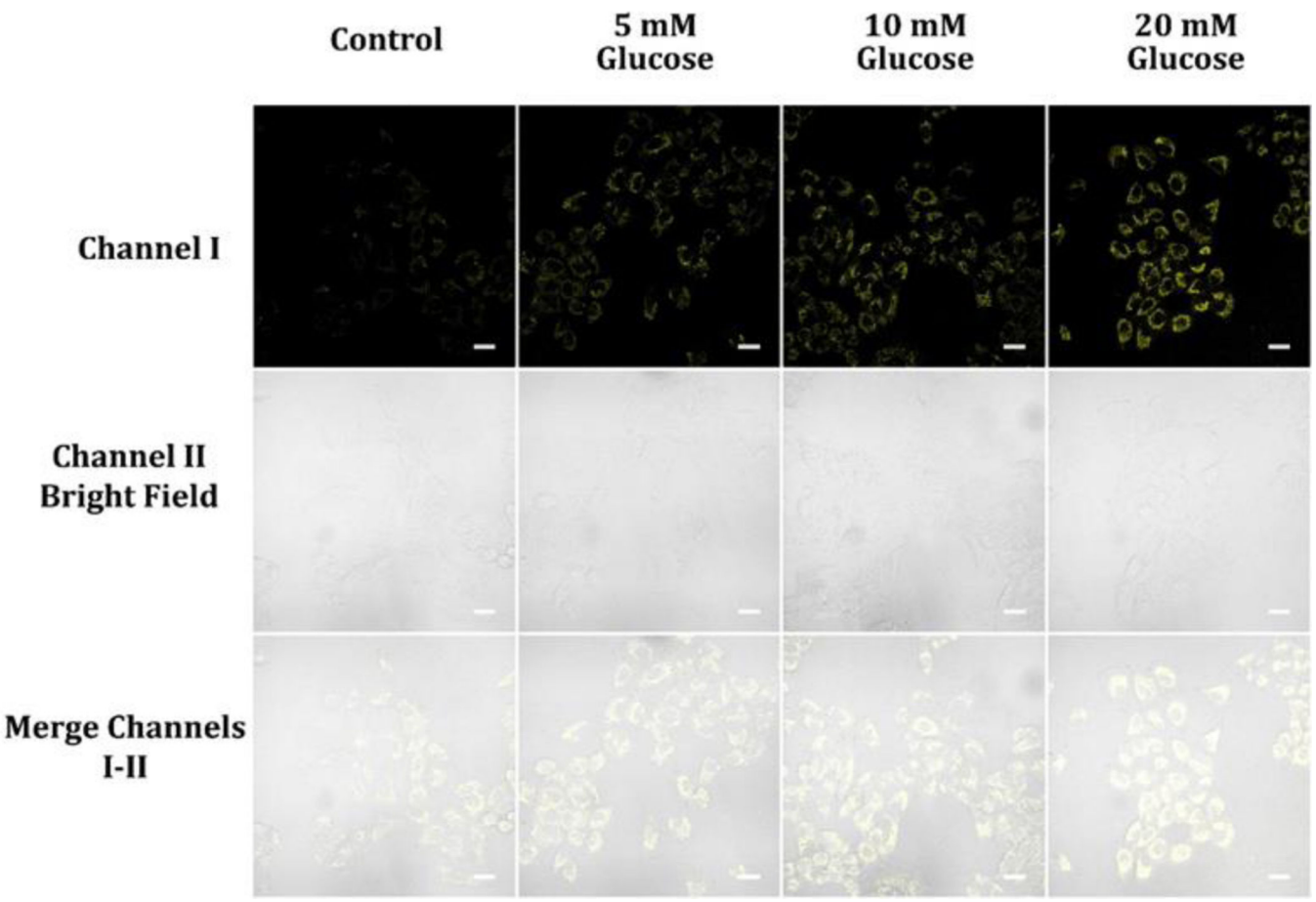

Figure 7.

Cellular luminescence images of A549 cells cultivated in DMEM medium containing 0, 5, 10, and 20 mM glucose for 30 min and subsequently treated with 10 μM probe **A** in glucose-deficient DMEM medium for 30 minutes. Image fluorescence signals were captured between 550 to 650 nm upon 488 nm excitation for both sets of images.

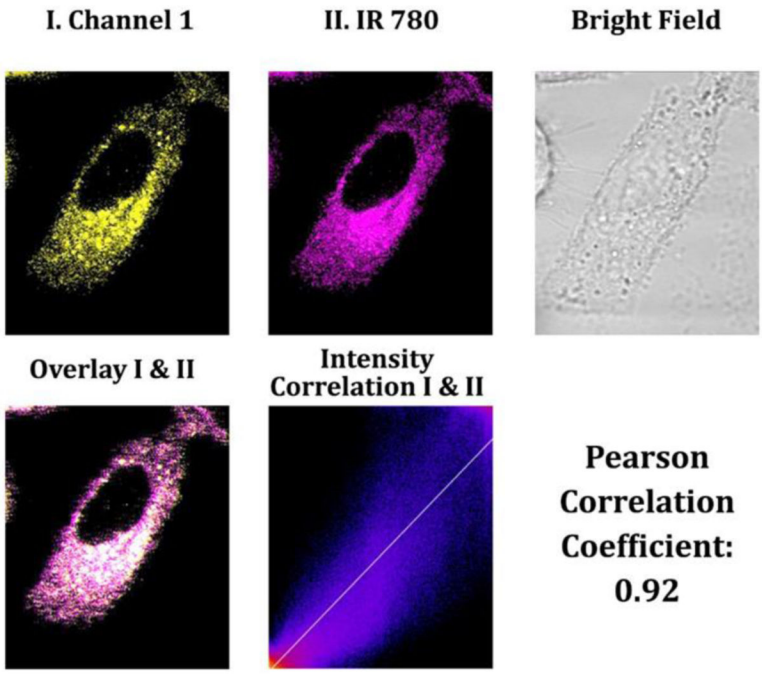

Figure 8.

Cellular luminescence images were captured of A549 cells that had been pretreated with 50 mM glucose in DMEM medium for 30 minutes, followed by co-incubation with 5 μM IR-780 cyanine dye and 10 μM probe **A** in glucose-free DMEM medium for 30 minutes. Yellow channel fluorescence images were gained employing 488 nm excitation and recorded between 550 and 650 nm. Additionally, magenta channel II was applied to capture near-infrared luminescence emitted from mitochondria-specific IR-780 cyanine dye between 750 and 800 nm under 635 nm excitation.

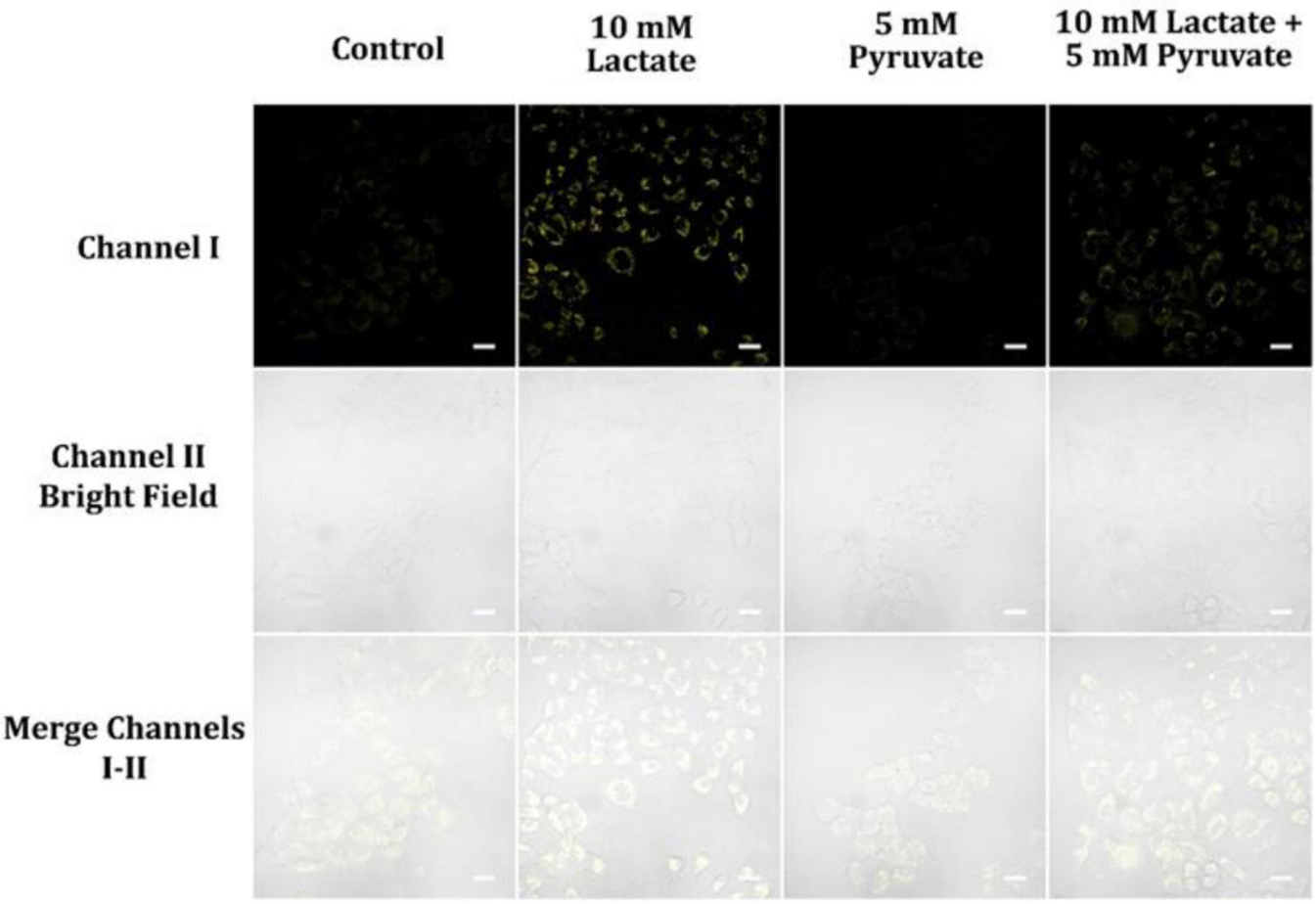

Figure 9.

Cellular luminescence images of A549 cells cultivated with 5 mM Pyruvate, 10 mM lactate, or a mixture of 5 mM pyruvate and 10 mM lactate in glucose-deficient DMEM medium for 30 min and then treated with 10 μM probe **A** in glucose-deficient DMEM medium for 30 minutes. The image fluorescence signals were gathered from 550 nm to 650 nm under 488 nm excitation.

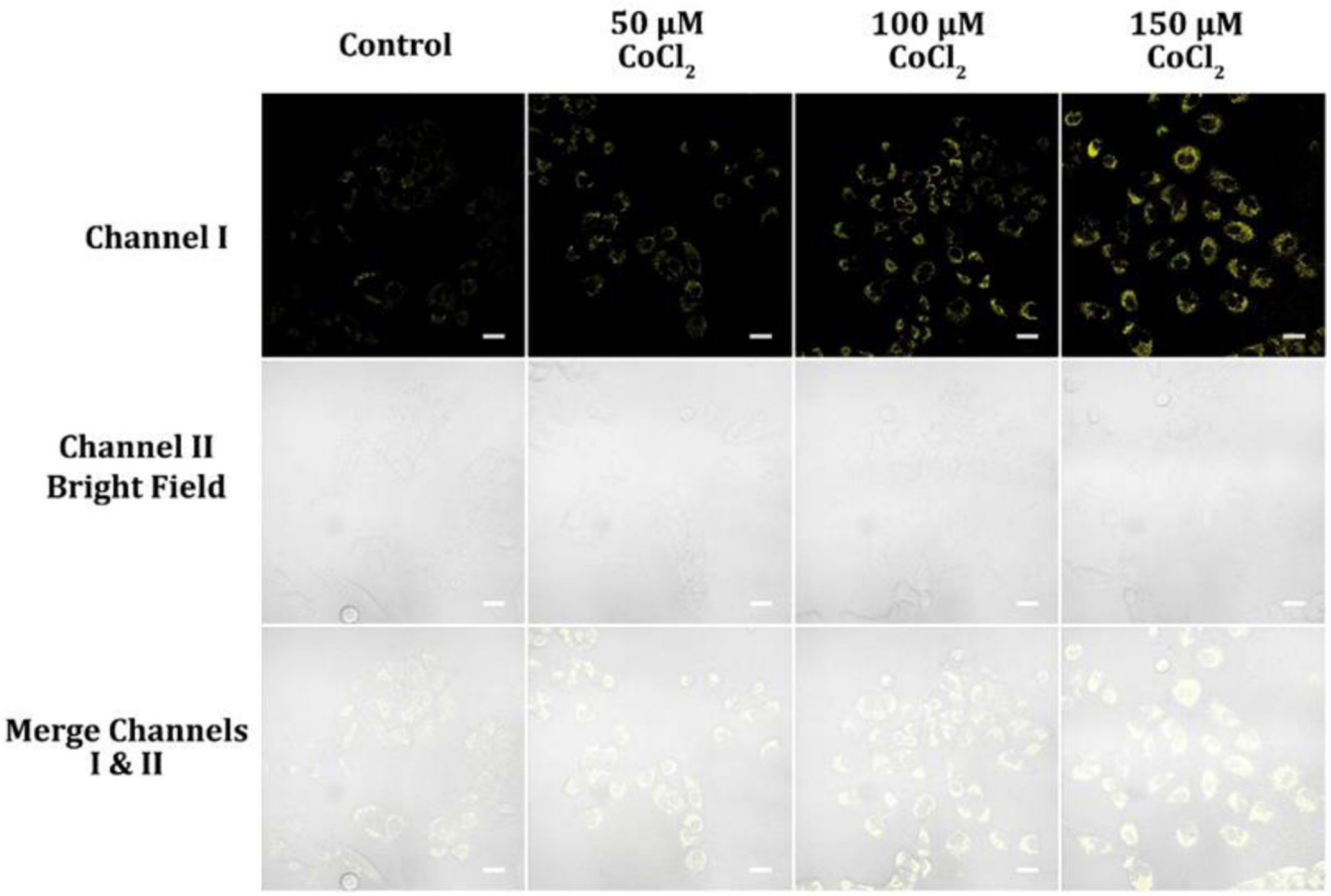

Figure 10.

Cellular luminescence images of A549 cells pre-treated with 50, 100, and 150 μM $CoCl_2$ in glucose-free DMEM medium for 12 hours and then cultivated in glucose-deficient DMEM medium holding 10 μM probe **A** for 30 minutes. The image fluorescence signals were obtained between 550 and 650 nm under 488 nm excitation.

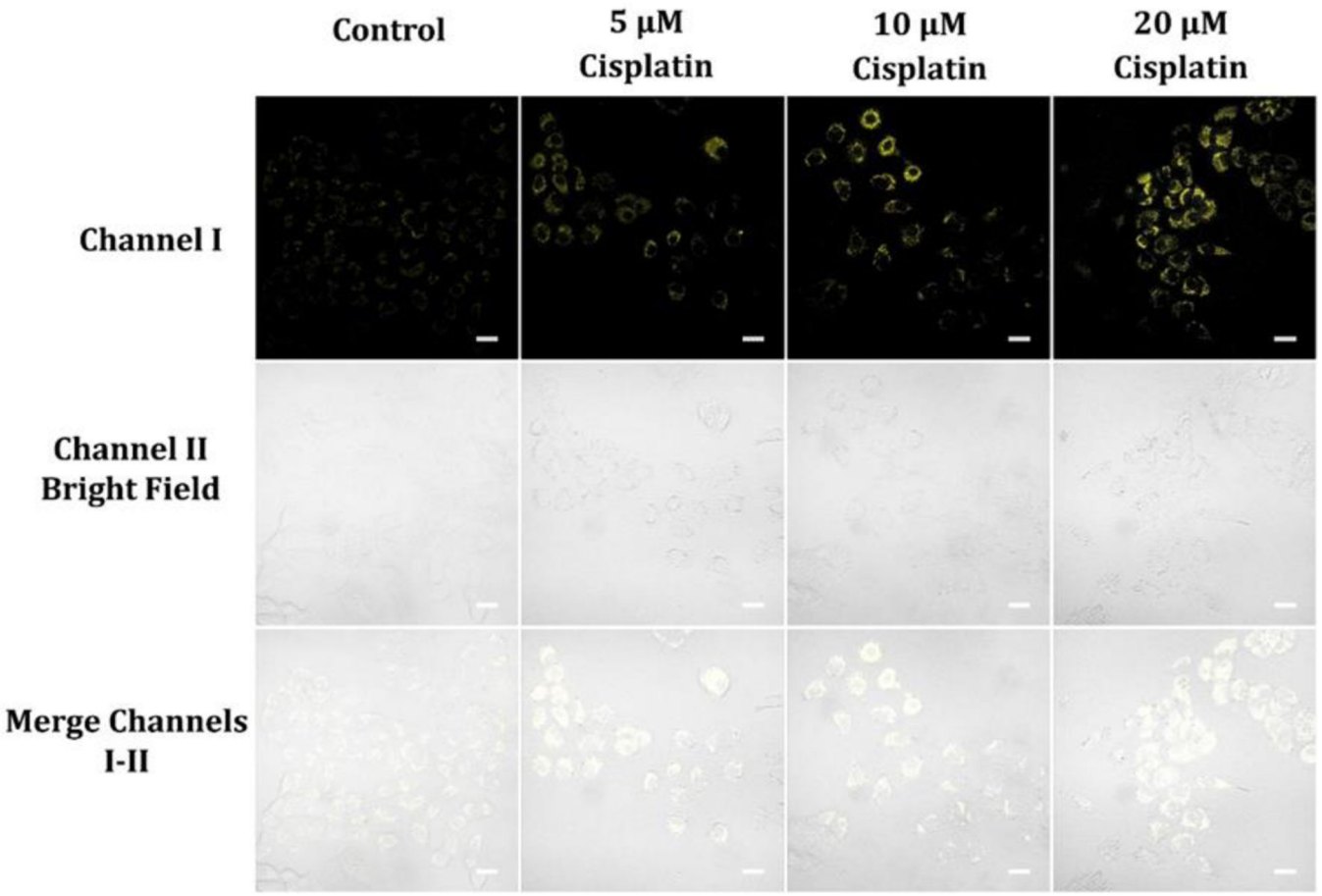

Figure 11.

Cellular luminescence images of A549 cells hatched in glucose-deficient DMEM medium containing 5, 10, and 20 μM cisplatin for 2 hours and then hatched with 10 μM probe **A** in glucose-deficient DMEM medium for 30 minutes. Image fluorescence signals were obtained between 550 nm and 650 nm under 488 nm excitation.

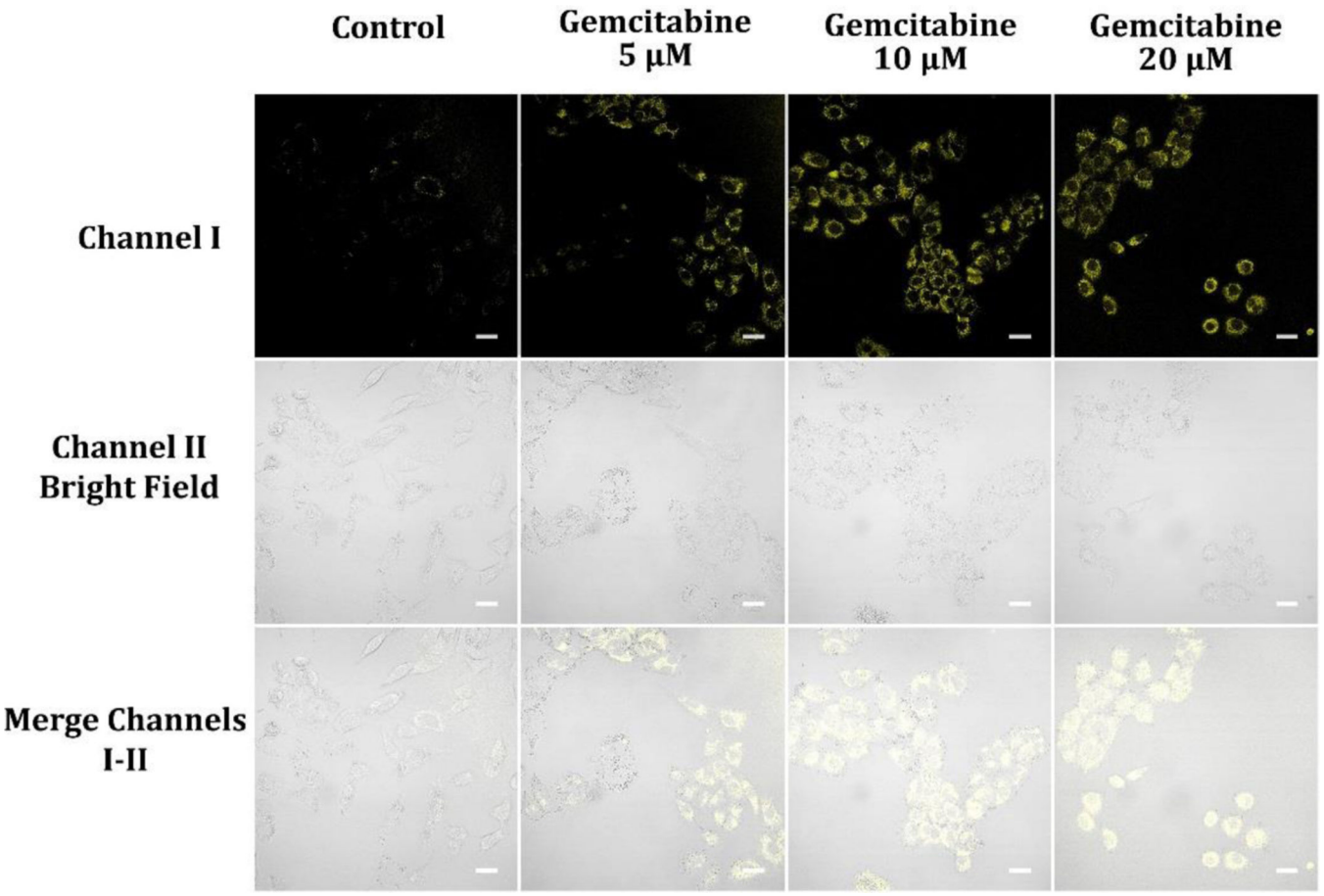

Figure 12.

Cellular luminescence images of A549 cells hatched in glucose-deficient DMEM medium holding 5, 10, and 20 μM gemcitabine for 2 hours and then cultivated in glucose-deficient DMEM medium holding 10 μM probe **A** for 30 minutes. Image fluorescence signals were obtained between 550 nm and 650 nm under 488 nm excitation.

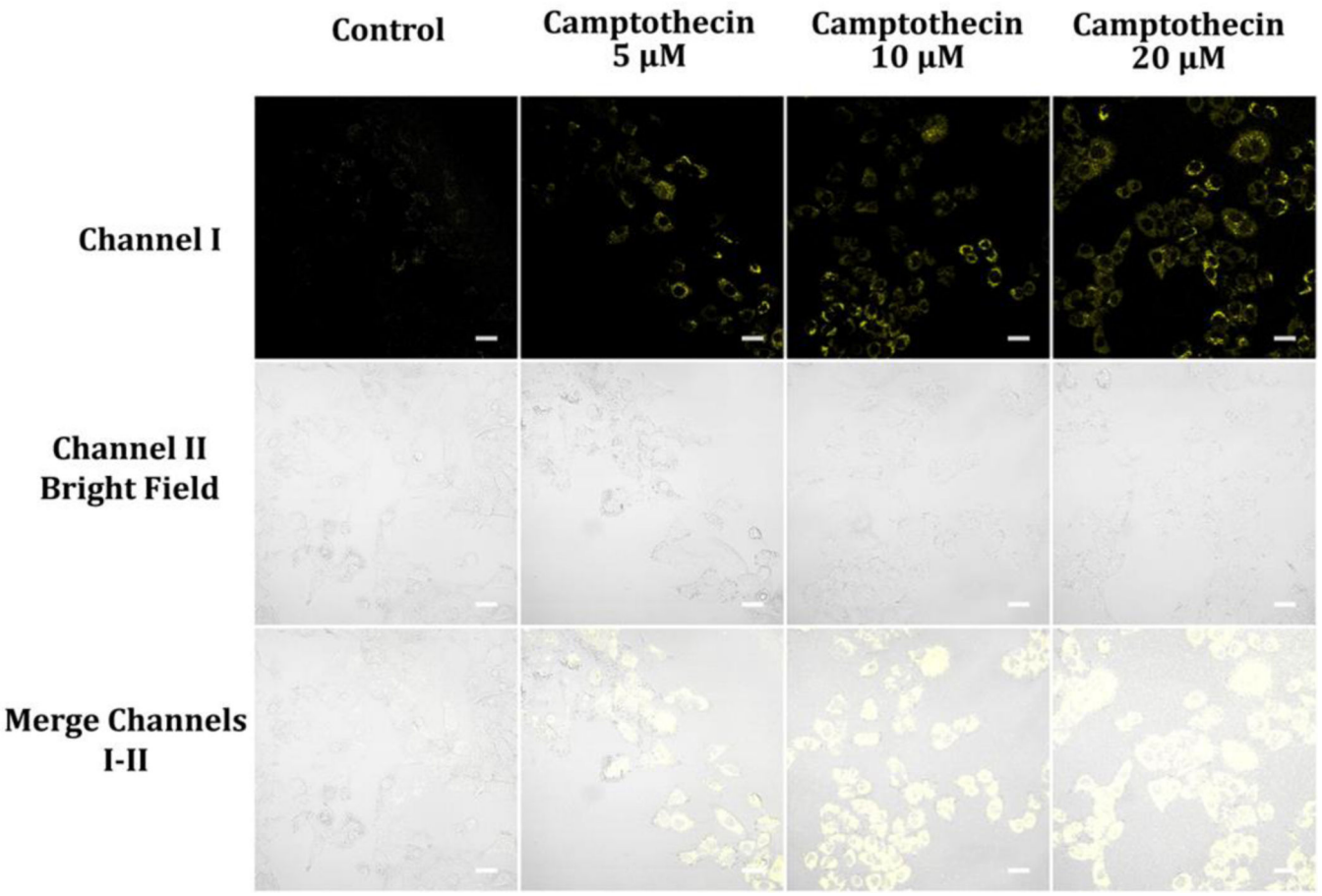

Figure 13.

Luminescence images of A549 cells hatched in glucose-deficient DMEM medium holding 5, 10, and 20 μM camptothecin for 2 hours and then cultivated in glucose-deficient DMEM medium including 10 μM probe **A** for 30 min. Image fluorescence signals were recorded from 550 nm to 650 nm under 488 nm excitation.

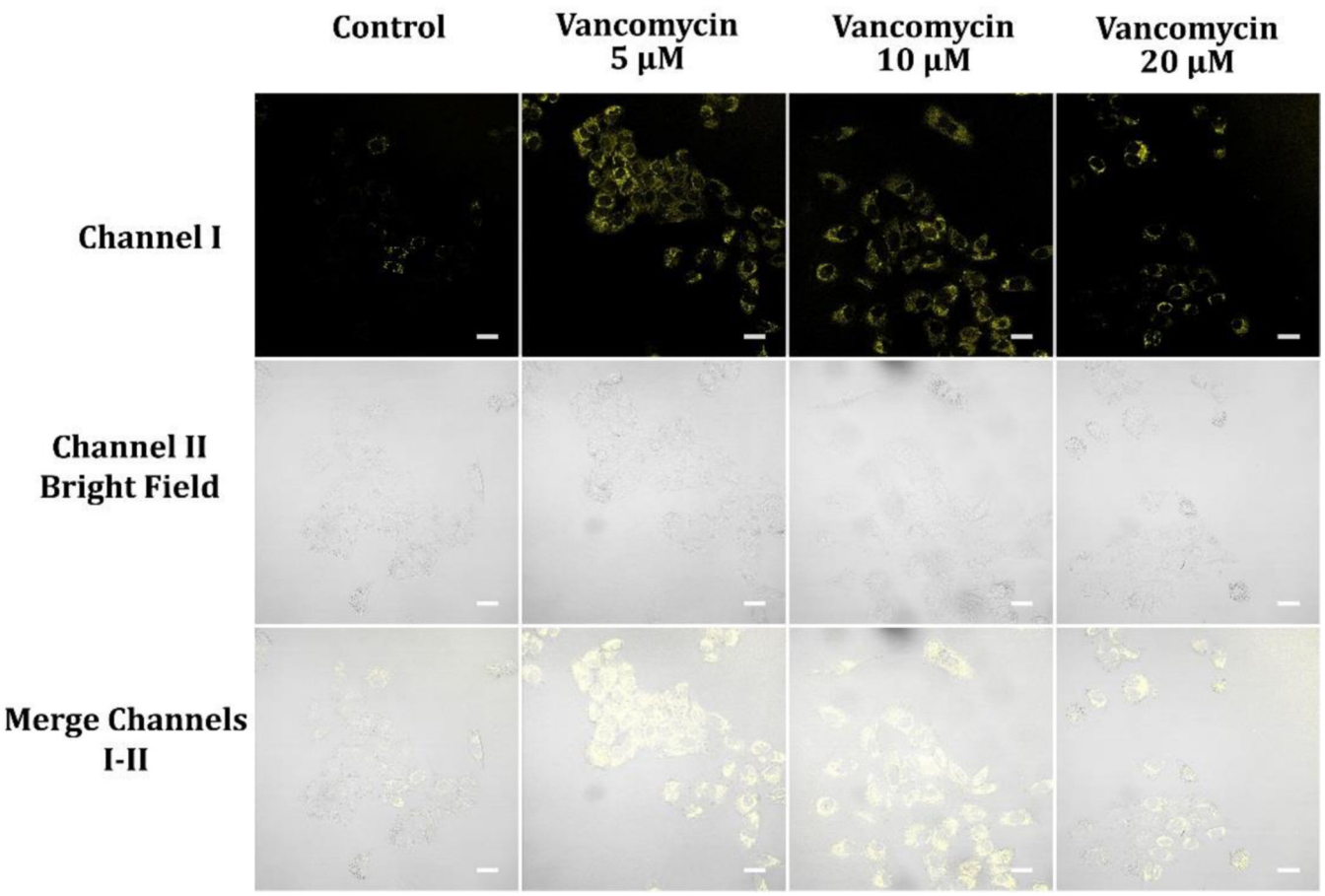

Figure 14.

Luminescence images of A549 cells preloaded with 5, 10, and 20 μM Vancomycin for 2 hours and then cultivated in glucose-deficient DMEM medium encompassing 10 μM probe **A** for 30 minutes. Image fluorescence signals were recorded from 550 nm to 650 nm under excitation at 488 nm.

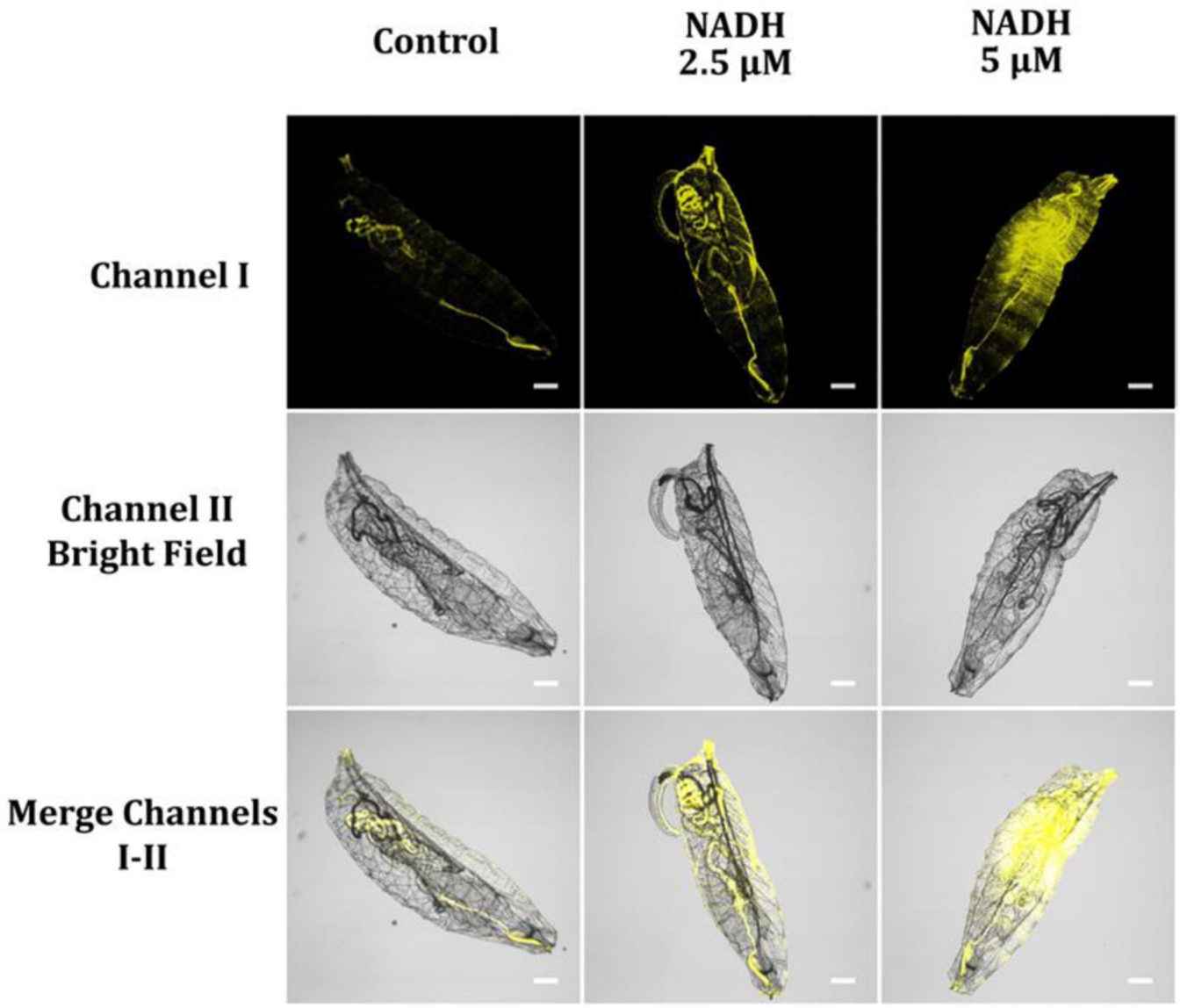

Figure 15.

Freshly starvation-hatched fruit fly larvae were placed in different NADH concentrations from 0 (control) to 5 μM in a pH 7.4 PBS buffer for 15 min, washed three times with the PBS buffer, and then immersed in PBS buffer solution holding 10 μM probe **A** for 30 minutes. Fluorescence signals from the images were obtained at a wavelength range of 550–650 nm upon 488 nm excitation.

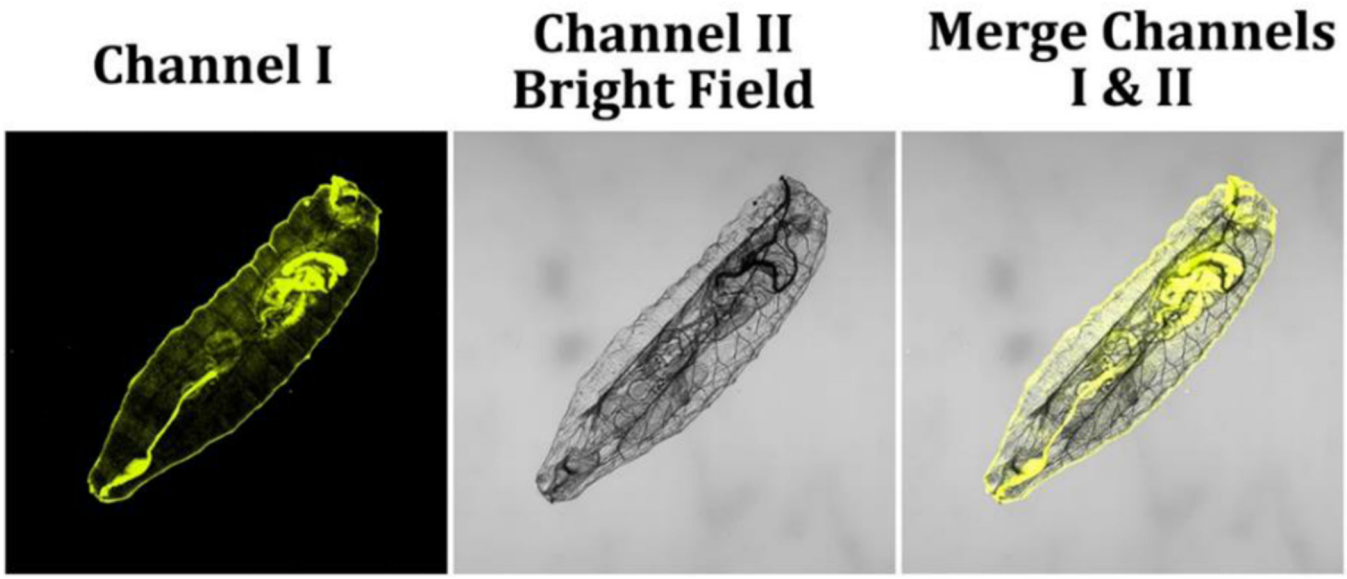

Figure 16.

Freshly food-hatched fruit fly larvae were immersed in pH 7.4 PBS buffer, including 10 μM probe **A** for 6 h, then washed thrice with the PBS buffer solution. Fluorescence signals from the image were collected at a wavelength range of 550–650 nm upon 488 nm excitation.